functional recovery, with BMS scores comparable to those of the chronic PBS group (Figure 6A).

The gait performance of the mice in each group was analyzed using the DigiGait system at 42 days after cell transplantation or PBS injection. In both PBS control groups and the chronic TP group, a subset of experimental animals (2 of 10 mice in each group) were unable to walk sufficiently well on a treadmill moving at 7 cm/s to perform the test, but all the mice in the sub-acute TP group could perform the test. Gait analysis revealed a significantly longer stride length in the sub-acute TP group than in the sub-acute PBS group, whereas no significant difference in stride length was detected between the chronic TP and either PBS group (Figure 6B). Consistent with these findings, in the Rotarod test at 42 days after cell transplantation or PBS injection, the mice in the sub-acute TP group remained on the rotating rod for a significantly longer time than those of the sub-acute PBS group, but no significant difference was observed between the chronic TP group and either PBS group (Figure 6C).

Electrophysiological examinations performed at 42 days after cell transplantation or PBS injection by motor-evoked potential (MEP). MEP waves were detected in all mice of the sub-acute TP group, and the average signal-to-response latency was 6.1 ± 0.2 ms and the average first wave amplitude was 134.0 ± 31.5 mv. However no MEP waves were observed at all in 5 out of the 7 mice in the chronic TP group and at all mice in the sub-acute and chronic PBS groups (Figure 6D). Taking the results of all the motor functional analyses together, no functional recovery of the hindlimbs was observed in the chronic TP group.

Discussion

Previous studies have indicated that NS/PC transplantation at the sub-acute phase has therapeutic potential for SCI [1-7,18]. At the chronic phase, however, NS/PC transplantation does not result in functional recovery. Many researchers have sought to improve motor function in chronic SCI by NS/PC transplantation. However,

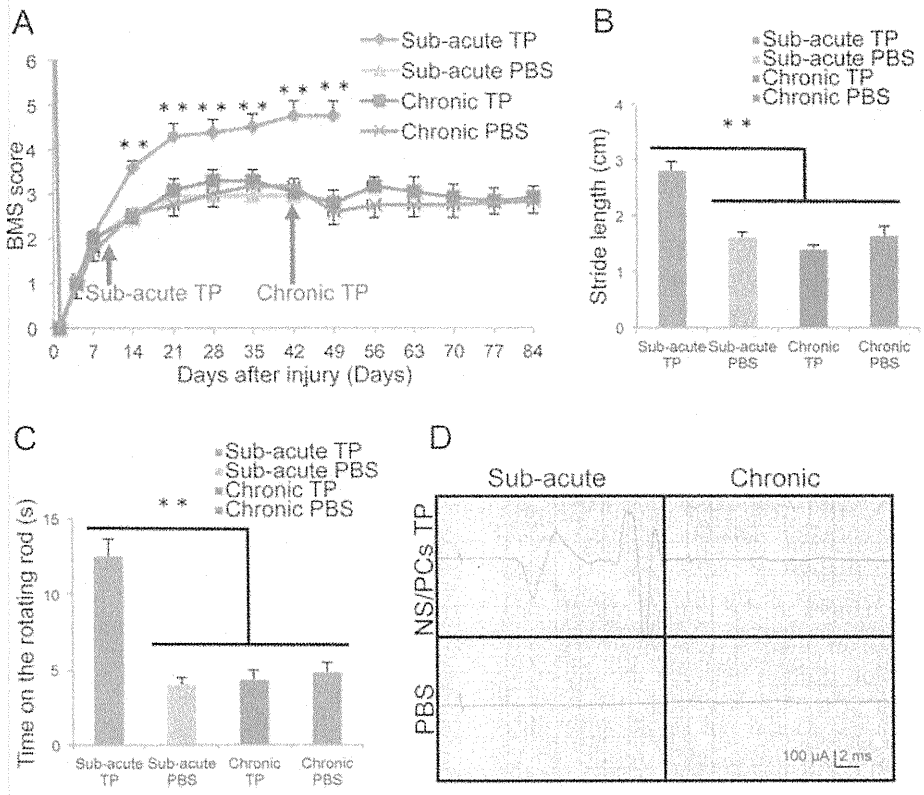

Figure 6 Motor function and electrophysiological recovery after NS/PC transplantation. **A**, Hindlimb motor function was assessed weekly by BMS score. The sub-acute TP group exhibited significantly better functional recovery than the vehicle control group at 14 DPI and thereafter, whereas no significant difference was observed between the chronic TP group and the vehicle control group. Values are means ± SEM (n = 10). $^{**}P < 0.01$. **B**, Treadmill gait analysis using the DigiGait system revealed a significantly longer stride in the sub-acute TP group than in the chronic TP group or either control group 42 days after cell transplantation or PBS injection. Values are means ± SEM (sub-acute TP n = 10, chronic TP and each control n = 8). $^{**}P < 0.01$. **C**, The sub-acute TP group walked for a significantly longer time on the rotating rod than the chronic TP group or either control group 42 days after cell transplantation or PBS injection. Values are means ± SEM (n = 10). $^{**}P < 0.01$. **D**, Representative profiles of MEP in the sub-acute TP, chronic TP, and both control groups 42 days after cell transplantation or PBS injection.

most studies obtained no significant functional recovery, and no consensus exists concerning the survival and/or fate of grafted cells in chronic-phase transplantation [9-12]. For example, some reports demonstrated that cells grafted at the chronic phase of SCI have a poor survival rate [9,12], while Cusimano et al. reported no significant difference in survival rate between NS/PC transplantation at the sub-acute versus the chronic phase [11]. However, these findings were based on histological examinations only. To clarify this issue, we performed sub-acute- and chronic-phase transplantations of NS/PCs derived from transgenic mice that ubiquitously express ffLuc-cp156 on a C57BL/6J background [14] to treat SCI in adult mice. These NS/PCs showed strong bioluminescent and fluorescent signals originating from ffLuc-cp156 [14], enabling the easy detection of surviving grafted cells in living animals noninvasively by BLI [4,13] and confirmation of integrated cells within the injured spinal cord by immunohistology for GFP without using a lentiviral vector.

Using cells from these mice, we demonstrated that the NS/PCs grafted during the chronic phase of SCI had a similar survival rate to those transplanted at the sub-acute phase. We also observed no significant difference between the two groups in the differentiation phenotypes of the grafted cells. The survival and/or differentiation potential of grafted cells can change remarkably due to microenvironmental changes in the injured spinal cord [19]. A previous study showed that grafted NS/PCs mainly differentiate into astrocytes after transplantation at the acute phase [4]. Inflammatory cytokines, such as IL-1β, IL-6, and TNF-α, also increase dramatically in the injured spinal cord during the acute phase [20,21], and these cytokines induce NS/PCs to differentiate into astrocytes. Moreover, growth factors affect the fate of grafted NS/PCs. For example, EGF, FGF, NT3, and PDGF have demonstrated beneficial effects on the survival of NS/PCs [10,12,22]. HGF and PDGF promote neuronal differentiation [23,24], whereas CNTF enhances glial differentiation *in vitro* [25]. To assess microenvironmental changes in the injured spinal cord, we performed a microarray analysis to exhaustively compare the gene expression profiles between the sub-acute and chronic phases of SCI. The expression levels of all cytokines and growth factors did not significantly differ, consistent with our BLI and histological results on the survival and/or fate of the grafted cells. These data suggested that the microenvironments of the injured spinal cord were not significantly different at the sub-acute and chronic SCI phases with respect to the expression of factors known to influence the survival rate and differentiation of grafted NS/PCs.

Many reports concern possible mechanisms underlying the therapeutic effects of NS/PC transplantation for SCI; for example, grafted cells contribute to the reconstruction of neural circuits and remyelination [2,6,17,26]. NS/PCs also secrete neurotrophic factors, which support the survival of host neural cells and enhance axonal growth and angiogenesis [27-30]. In this study, motor function recovery was observed in the sub-acute TP group, but not in the chronic TP group. Consistent with this result, more NF-H$^+$ neuronal fibers and 5HT$^+$ serotonergic fibers, which are involved in motor function recovery [30-32], were observed in the sub-acute TP group than in the sub-acute PBS group. Moreover, Luxol Fast Blue (LFB) staining revealed significantly larger myelinated areas in the sub-acute TP group than in the sub-acute PBS group. By contrast, no significant differences in NF-H$^+$ neuronal fibers, 5HT$^+$ serotonergic fibers, or LFB$^+$ myelinated areas were observed between the chronic TP and chronic PBS groups. Furthermore, no MEP waves were detected in most mice in the chronic TP group.

As a possible reason for these findings, we refer to the poor migration of grafted cells in the chronic TP group. Since glial scar formation prevented grafted NS/PCs from migrating away from the graft site and integrating with the host spinal cord, the regeneration of neural circuits, remyelination, and/or preservation of host neural cells did not occur in areas rostral and caudal to the injured spinal cord of the chronic TP group. Consistent with this scenario, many previous reports indicate that insufficient migration of grafted cells results in poor functional recovery after SCI [33,34].

Our microarray and histological analyses suggested that more macrophages or microglial cells, including a substantial number of M2 macrophages, were distributed around the lesion epicenter at the sub-acute phase than at the chronic phase. In agreement with this finding, previous studies have reported that infiltration of macrophages and microglial cells peaks at approximately 7 DPI [35,36]. Moreover, M2 macrophages have an anti-inflammatory role and promote axonal growth after SCI [37-39], and their phagocytic activity was shown to contribute to tissue repair in the injured CNS by reducing myelin debris [40-42]. In addition, Busch et al. demonstrated that activated macrophages induced axonal dieback in the injured CNS [43], which was prevented by switching the infiltrating macrophages from M1 to M2 phenotype [39]. Furthermore, grafted NS/PCs also exert immunomodulatory effects through interactions with infiltrating immune cells [44,45]. Especially in the sub-acute phase, grafted NS/PCs can affect the properties of infiltrating macrophages, inducing their shift from M1 to M2 in the injured spinal cord [11,39]. Therefore, NS/PCs transplanted at the sub-acute stage may alter the microenvironment to favor M2, resulting in a synergistic effect that supports the increase in neuronal fibers and

functional recovery. These findings indicate that a novel immunomodulatory strategy, such as the administration of a mediator of phenotypic switching from M1 to M2 or the combined transplantation of NS/PCs and M2 macrophages, may have therapeutic potential in chronic SCI. In contrast, previous studies reported that M1 macrophages impairs recovery of SCI through the production of oxidative metabolites or pro-inflammatory cytokines including TNF-α, which induced the apoptotic cell death of neural precursor cells [42,46,47]. However, the expressions of genes associated with M1 macrophages showed no significant difference among the subacute and chronic phases. These findings are consistent with the similar survival rate of the grafted NS/PCs in both TP groups.

Taken together, these results suggest that during the chronic phase of SCI, the injured spinal cord microenvironment appears to be unfavorable for the therapeutic mechanisms of NS/PC transplantation, owing to extensive glial scarring [48] and/or the phenotype of infiltrating macrophages. Accordingly, to improve the therapeutic potential of NS/PC transplantation performed at the chronic phase, altering the microenvironment in the injured spinal cord is likely to be important. For example, suppression of axonal growth inhibitors may improve the microenvironment. CSPGs, which are the most prevalent axonal growth inhibitors, are produced by reactive astrocytes and involved in glial scarring [48]. Chondroitinase ABC (ChABC), which digests CSPG, promotes axonal growth and the migration of grafted NS/PCs [49,50]. Karimi-Abdolrezaee et al. described that CSPGs hinder the survival of grafted cells and the combined therapy of ChABC administration and NS/PCs transplantation promotes the migration and integration of grafted cells [51]. While our data demonstrated that CSPGs prevent the migration of grafted cells, but show no influence on their survival, we have great hopes that a combination of NS/PC transplantation and the administration of a suppressor of axonal growth inhibitor may be effective for inducing functional recovery in chronic SCI.

Conclusions

Microenvironmental changes in SCI affect the survival and/or fate of NS/PCs grafted into the injured spinal cord. The survival rate and differentiation phenotype of grafted cells were similar between chronic-phase and sub-acute-phase transplantation, with no significant difference in the secretion of cytokines and growth factors in the host environment between the two phases. However, the distribution of grafted cells was restricted by the robust glial scar that formed around the lesion epicenter at the chronic phase. Consequently, no functional recovery was observed in this phase. Additionally, in the sub-acute phase, M2 macrophages, which infiltrated predominantly in this phase, might contribute to the functional repair upon NS/PC transplantation. Alteration of the microenvironment in SCI, focusing on the glial scar and the inflammatory phenotype, appears to be the best possible solution to maximize the therapeutic potential of NS/PC transplantation in the chronic phase.

Methods

NS/PC culture and analysis

NS/PCs were cultured and expanded, as previously reported [52]. Briefly, the striata of transgenic mice ubiquitously expressing ffLuc-cp156, a fusion protein of firefly luciferase and a circularly permuted Venus protein [14], were dissociated using a fire-polished glass pipette on embryonic day 14. Venus is a fluorescent protein with fast and efficient maturation that was originally engineered from GFP [53], and therefore grafted cells can be detected as fluorescent Venus signals using anti-GFP antibody [17,26]. Dissociated cells were collected by centrifugation and re-suspended in culture medium, which consisted of Dulbecco's modified Eagle medium/F12 (Sigma-Aldrich, St. Louis, MO, USA) supplemented with a previously described hormone mixture [52]. Human recombinant FGF-2 (Peprotech, Rocky Hill, NJ, USA) and EGF (Peprotech) (20 ng/ml each) were added every 2 days. The cells formed floating cell clusters (neurospheres) within 2–3 days. After propagation for 3 passages, the neurospheres were used for *in vitro* BLI, differentiation, and proliferation assays, and for cell transplantation.

For differentiation analysis, the neurospheres were plated onto poly-L-ornithine/fibronectin-coated 8-well chamber slides (Iwaki; Asahi Glass Co Ltd., Tokyo, Japan) at a density of 1×10^5 cells/ml and cultured in culture medium without serum or growth factors at 37°C in 5% CO_2 and 95% air for 7 days. The differentiated cells were then fixed with 4% paraformaldehyde in 0.1 M PBS and stained with the following primary antibodies for immunocytochemistry: anti-Tuj-1 (mouse IgG, 1:1000, Sigma-Aldrich), anti-GFAP (rat IgG, 1:1000, Invitrogen, Carlsbad, CA, USA), and anti-CNPase (mouse IgG1, 1:1000, Sigma-Aldrich). Nuclei were stained with Hoechst 33258 (10 μg/ml, Sigma-Aldrich). *In vitro* images were obtained using a fluorescence microscope (BZ-9000; Keyence Co., Osaka, Japan).

The proliferation assay was performed by measuring ATP, which indirectly reflects the number of viable cells [15,17,54]. In brief, NS/PCs were first incubated in culture medium without serum or growth factors in 48-well cell-culture plates (Corning Inc., Corning, NY, USA) at 37°C in 5% CO_2 and 95% air for 24 or 72 h. D-luciferin was then added to each well, and the luminescent signal was detected immediately using a Xenogen-IVIS spectrum cooled charged-coupled device (CCD) optical macroscopic imaging system (Caliper Life

Sciences, Hopkinton, MA, USA). To determine the population doubling time, the ATP assay was modified, as described elsewhere [15,17,54].

SCI model

Adult female C57BL/6J mice (8–10 weeks old, 18–22 g, n = 52; Clea, Tokyo, Japan) were anesthetized with an intraperitoneal (i.p.) injection of ketamine (100 mg/kg) and xylazine (10 mg/kg). After laminectomy at the 10th thoracic spinal vertebra (Th10), the dorsal surface of the dura mater was exposed. Contusive SCI was induced using a commercially available SCI device (IH Impactor, Precision Systems and Instrumentation, Lexington, KY, USA), as previously described [4]. This device creates a reliable contusion injury by rapidly applying a force-defined impact (60 kdyn) with a stainless steel-tipped impactor. All experiments were approved by the ethics committee of Keio University and fully in accordance with the Guide for the Care and Use of Laboratory Animals (National Institutes of Health, Bethesda, MD, USA).

Microarray analysis

The injured mice were anesthetized and transcardially perfused with heparinized saline (5 U/ml) at 9 DPI or 42 DPI (n = 3 each). Dissected segments of spinal cord at the Th10 level were rapidly frozen and placed in TRIzol (Invitrogen). Total RNA was isolated using an RNeasy Mini Kit (Qiagen Inc., Hilgen, Germany), in accordance with the manufacturer's instructions. As a control, samples of naïve spinal cord were harvested by the same protocol. For microarray analysis, RNA quality was assessed using a 2100 Bioanalyzer (Agilent Technologies Inc., Santa Clara, CA, USA), and 100 ng of total RNA was reverse transcribed, biotin labeled, and hybridized to a GeneChip® Mouse Genome 430 2.0 Array (Affymetrix Inc., Santa Clara, CA, USA). The array was then washed and stained in a Fluidics Station 450, according to the manufacturer's instructions [55,56]. The microarrays were scanned using a GeneChip Scanner 3000 7G, and the raw image files were converted to normalized signal intensity values using the MAS 5.0 algorithm. PCA was carried out with Gene Spring GX software (Agilent Technologies Inc.), using the full set of normalized data. For the clustering analysis, the normalized data were narrowed down by the cut-off values of expression levels (>50) and by fold change (>1.5, versus the signal of intact spinal cord), and statistical analysis was performed using one-way ANOVA followed by the Tukey-Kramer test ($P < 0.05$). The heat map was visualized with Gene Spring GX.

NS/PC transplantation

Various numbers of NS/PCs (approximate range 2.5×10^4 to 5×10^5 cells/2 μl) were transplanted into uninjured naïve mice (n = 3, each), and NS/PCs (5×10^5 cells/2 μl) were transplanted at 9 DPI (sub-acute TP group, n = 10) or 42 DPI (chronic TP group, n = 10) as previously reported [4,16,17,26,30,57]. The NS/PCs were transplanted into the lesion epicenter with a glass micropipette at a rate of 1 μl/min using a Hamilton syringe (25 μl) and a stereotaxic microinjector (KDS 310, Muromachikikai Co. Ltd., Tokyo, Japan). PBS (2 μl) was similarly injected into the lesion epicenter of the control mice at each time point (sub-acute and chronic PBS groups, n = 10 each).

Bioluminescence imaging

A Xenogen-IVIS spectrum CCD optical macroscopic imaging system was used for *in vitro* and *in vivo* BLI as previously reported [4,16,17]. In brief, the signal intensity of NS/PCs *in vitro* was assessed using plated cells at various cell numbers (approximate range 1×10^2 to 1×10^4 cells/well), and BLI was performed immediately after adding D-luciferin (150 μg/ml) (n = 3). The integration time was fixed at 1 min for each image.

In vivo imaging was performed 15 min after the i.p. injection of D-luciferin (0.3 mg/g body weight) with the field-of-view set at 13.2 cm, because the photon count was most stable during this period. The intensity peaked between 10 and 30 min after the i.p. injection of D-luciferin. The integration time was fixed at 5 min for each image. All images were analyzed with Living Image software (Caliper Life Sciences), and the optical signal intensity was expressed as photon flux (photon count) in units of photons/s/cm^2/steradian. Each result was displayed as a pseudo-colored photon count image superimposed on a gray-scale anatomic image. To quantify the measured light, a region of interest was defined in the cell-implanted area, and all values at the same region of interest were examined.

Behavioral analyses

The motor function of each mouse was evaluated weekly using the BMS up to 49 DPI in the sub-acute TP and PBS groups and up to 84 DPI in the chronic TP and PBS groups (n = 10 per group) [58]. This assessment was performed by two investigators blinded to the identity of the experimental mice.

Motor coordination was evaluated using a rotating rod apparatus (Rotarod, Muromachikikai Co., Ltd.), which consisted of a plastic rod (3 cm diameter, 8 cm length) with a gritted surface flanked by two large discs (40 cm diameter) (n = 10 per group). At 42 days after cell transplantation or PBS injection, each mouse was placed on the rod while it rotated at 20 rpm for 2 min sessions [59]. Three trials were conducted, and the maximum number of seconds the mouse stayed on the rod was recorded.

Gait analysis was performed using the DigiGait system (Mouse Specifics, Quincy, MA, USA) (n = 10 per group) [17,26,60]. Each mouse demonstrated weight-supported hindlimb stepping at 42 days after cell transplantation or PBS injection. The stride length was determined on a treadmill set to a speed of 7 cm/s.

Electrophysiology

Electrophysiological experiments were performed using a Neuropack S1 MEB-9402 (Nihon Kohden, Tokyo, Japan) at 42 days after cell transplantation or PBS injection (n = 7 per group) [26]. The animals were anesthetized with an i.p. injection of ketamine (60 mg/kg) and xylazine (6 mg/kg), and the stimulation was applied through the occipitocervical area of the spinal cord and the hindlimb by needle electrodes. The active electrode was placed in the quadriceps muscle belly, and the reference electrode was placed near the distal quadriceps tendon. The ground electrode was placed on the tail. A stimulus of 0.4 mA intensity, 0.2 ms duration, and 1 Hz interstimulus interval were used. The latency was measured as the length of time from the stimulus to the onset of first response wave. The amplitude was measured from the initiation point of the first response wave to its highest point.

Histological analyses

Injured animals were deeply anesthetized and transcardially perfused with 4% PFA in 0.1 M PBS at 9 DPI or 42 DPI (n = 3 each). The treated animals were similarly prepared 42 days after cell transplantation or PBS injection. The spinal cords were removed, postfixed overnight in 4% PFA, soaked overnight in 10% sucrose, followed by 30% sucrose, embedded in Optimal Cutting Temperature compound (Sakura Finetechnical Co., Ltd., Tokyo, Japan), frozen, and sectioned in the sagittal or axial plane at 12 μm thickness on a cryostat (CM3050 S; Leica Microsystems, Wetzlar, Germany). The injured spinal cord sections were histologically evaluated by HE staining and immunohistochemistry, followed by quantitative analysis. The sections of transplanted spinal cord were subjected to HE staining, LFB staining, and immunohistochemistry followed by quantitative analyses.

For immunohistochemistry, tissue sections were stained with the following primary antibodies: anti-GFP (rabbit IgG, 1:200; Frontier Institute, Hokkaido, Japan), anti-Hu (human IgG, 1:1000, a gift from Dr. Robert Darnell, The Rockefeller University, New York, NY, USA), anti-GFAP (rat IgG, 1:200, Invitrogen), anti-APC CC-1 (mouse IgG, 1:200; Calbiochem, San Diego, CA, USA), anti-nestin (mouse IgG1, 1:500; BD Bioscience Pharmingen, San Jose, California, USA), anti-CS56 (a marker for CSPG, mouse IgM, 1:200; Sigma-Aldrich), anti-Iba1 (a marker for microglia/macrophages, rabbit IgG, 1:200; Wako Pure Chemical Industries, Osaka, Japan), anti-arginase-1 (a marker for M2 macrophages, goat IgG, 1:200; Santa Cruz Biotechnology, Santa Cruz, CA, USA), anti-LAMP2 (a marker for endosomes or lysosomes, rat IgG, 1:200; Abcam, Cambridge, UK), anti-NF-H (mouse IgG1, 1:200; Chemicon, Millipore, Billerica, MA, USA), and anti-5HT (goat IgG, 1:200; Immunostar, Hudson, WI, USA). For immunohistochemistry with anti-GFP, -NF-H, and -5HT, a biotinylated secondary antibody (Jackson Immunoresearch Laboratory Inc., West Grove, PA, USA) was used after exposing the sections to 0.3% H_2O_2 for 30 min at room temperature to inactivate endogenous peroxidases. The signals were enhanced with the Vectastain ABC kit (Vector Laboratories, Inc., Burlingame, CA, USA). Nuclei were stained with Hoechst 33258 (10 μg/ml, Sigma-Aldrich). All images were obtained using a fluorescence microscope (BZ 9000; Keyence Co.) or a confocal laser scanning microscope (LSM 700; Carl Zeiss, Munich, Germany).

Quantitative analyses

Quantitative analyses of the histological findings (HE, LFB staining, and immunostaining for CS56, Iba1, NF-H, 5HT, GFP/each phenotypic marker, and arginase-1/Iba1) were performed using a BZ 9000 microscope and Dynamic Cell Count BZ-HIC software (Keyence Co.). The threshold values were maintained at a constant level for all analyses. The GFP^+ area was quantified using images of axial sections of the lesion epicenter and 0.5 mm, 1.0 mm, 2.0 mm, 3.0 mm, and 4.0 mm rostral and caudal to the epicenter at 100× magnification (n = 4 each). To determine the spinal cord area, HE-stained images of axial sections of the lesion epicenter and 4.0 mm rostral and caudal to the epicenter at 100× magnification were used (n = 3 each). Quantitative analysis of the LFB^+ area was similarly performed using axial sections of the lesion epicenter and 4.0 mm rostral and caudal to the epicenter at 100× magnification (n = 3 each). $CS56^+$ areas as well as $Iba1^+$ areas were quantified in the midsagittal sections of injured spinal cords at 100× magnification (n = 3 each).

To quantify $NF\text{-}H^+$ fibers, four regions were automatically captured within the midsagittal sections of the lesion epicenter and 4.0 mm rostral and caudal to the epicenter at 400× magnification (n = 3 each). To assess the $5HT^+$ fibers, five automatically captured regions within the axial sections were analyzed at the lumbar intumescence, which was 6–8 mm caudal to the lesion epicenter (n = 3 each).

To quantify the proportion of each cell phenotype among the grafted cells *in vivo*, five regions were captured within sagittal sections at 200× magnification using an LSM 700 confocal laser scanning microscope. GFP and phenotypic marker double-positive cells were counted in each section (n = 3 each). To quantify the infiltrated M2 macrophages in the injured spinal cord,

the number of Iba1 and arginase-1 double-positive cells was counted within five regions of sagittal sections of the lesion epicenter at 200× magnification with an LSM 700 confocal laser scanning microscope (n = 3 each).

Statistical analysis

All data are reported as the mean ± SEM. An unpaired two-tailed Student's *t* test was used to evaluate the differences between groups with respect to microarray gene expression profile, *in vivo* BLI analysis, *in vivo* differentiation assays, and analyses of the CS56$^+$, Iba1$^+$ and GFP$^+$ areas, and arginase-1$^+$/Iba1$^+$ cells. One-way ANOVA followed by the Tukey-Kramer test for multiple comparisons was used in the analyses of the HE, LFB, NF-H$^+$, and 5HT$^+$ areas and the Rotarod and DigiGait results. Repeated-measures two-way ANOVA followed by the Tukey-Kramer test was used for the BMS analysis. *P* values < 0.05 were considered statistically significant.

Abbreviations

NS/PCs: Neural stem/progenitor cells; SCI: Spinal cord injury; DPI: Days post-injury; BLI: Bioluminescence imaging; TP group: Transplanted group; ffLuc: Fluorescent protein-fused luciferase; Tuj-1: βIII tubulin; GFAP: Glial fibrillary acidic protein; CNPase: 2'3'-cyclic nucleotide 3'-phosphodiesterase; CSPG: Chondroitin sulfate proteoglycan; PCA: Principal component analysis; iNOS: Inducible nitric oxide synthase; APC: Adenomatous polyposis coli antigen; HE: Hematoxylin-eosin; PBS: Phosphate-buffered saline; NF-H: 200 kDa neurofilament; 5HT: 5-hydroxytryptamine; BMS: Basso Mouse Scale; MEP: Motor-evoked potential; LFB: Luxol Fast Blue; ChABC: Chondroitinase ABC.

Competing interests

The authors have declared that no competing interests exist.

Authors' contributions

SN, AY, OT, HO, and MN designed the research; SN, AY, HI, MT, and HE performed research; SN, AY, and HI analyzed the data; SN, HO, and MN wrote the paper; and MN and HO supervised all the experiments. All authors read and approved the final manucript.

Acknowledgments

We appreciate the help of Dr. A. Iwanami, Dr. Y. Takahashi, Dr. M. Shinozaki, Dr. T. Konomi, Dr. R. Zhang, Dr. G. Itakura, Dr. S. Tashiro, Dr. S. Kawabata, Dr. Y. Nishiyama, and Dr. K. Hori, members of the spinal cord research team at the Department of Orthopaedic Surgery, Rehabilitation Medicine and Physiology, Keio University School of Medicine. We also thank Ms. T. Harada, Ms. S. Miyao, Ms. M. Mizutani, and Ms. H. Shimada for their assistance with the experiments and animal care.

This work was supported by grants from the Japan Science and Technology–California Institute for Regenerative Medicine collaborative program; Grants-in-Aid for Scientific Research from the Japan Society for the Promotion of Science (SPS) and the Ministry of Education, Culture, Sports, Science, and Technology of Japan (MEXT); the Project for Realization of Regenerative Medicine; Support for Core Institutes for iPS Cell Research from the MEXT; Keio Gijuku Academic Development Funds; by a Grant-in-Aid for the Global COE program from MEXT to Keio University; and by a Grant-in-Aid for Scientific Research on Innovative Areas (Comprehensive Brain Science Network) from the MEXT.

Author details

[1]Department of Orthopaedic Surgery, 35 Shinanomachi, Shinjuku, Tokyo 160-8582, Japan. [2]Department of Physiology, Keio University School of Medicine, 35 Shinanomachi, Shinjuku, Tokyo 160-8582, Japan. [3]Department of Orthopaedic Surgery, Saitama Social Insurance Hospital, 4-9-3 Kitaurawa, Urawa, Saitama 330-0074, Japan. [4]Department of Orthopaedic Surgery, Murayama National Hospital Organization Murayama Medical Center, 2-37-1 Gakuen, Musashimurayama, Tokyo 208-0011, Japan. [5]Genomic Science Laboratories, Dainippon Sumitomo Pharma Co, Ltd., 2-6-8 Doshoumachi, Chuo, Osaka 541-0045, Japan.

Received: 27 November 2012 Accepted: 25 December 2012
Published: 8 January 2013

References

1. Ogawa Y, Sawamoto K, Miyata T, Miyao S, Watanabe M, Nakamura M, Bregman BS, Koike M, Uchiyama Y, Toyama Y, Okano H: **Transplantation of in vitro-expanded fetal neural progenitor cells results in neurogenesis and functional recovery after spinal cord contusion injury in adult rats.** *J Neurosci Res* 2002, **69**:925–933.
2. Cummings BJ, Uchida N, Tamaki SJ, Salazar DL, Hooshmand M, Summers R, Gage FH, Anderson AJ: **Human neural stem cells differentiate and promote locomotor recovery in spinal cord-injured mice.** *Proc Natl Acad Sci USA* 2005, **102**:14069–14074.
3. Hofstetter CP, Holmström NAV, Lilja JA, Schweinhardt P, Hao J, Spenger C, Wiesenfeld-Hallin Z, Kurpad SN, Frisén J, Olson L: **Allodynia limits the usefulness of intraspinal neural stem cell grafts; directed differentiation improves outcome.** *Nat Neurosci* 2005, **8**:346–353.
4. Okada S, Ishii K, Yamane J, Iwanami A, Ikegami T, Katoh H, Iwamoto Y, Nakamura M, Miyoshi H, Okano HJ, Contag CH, Toyama Y, Okano H: **In vivo imaging of engrafted neural stem cells: its application in evaluating the optimal timing of transplantation for spinal cord injury.** *FASEB J* 2005, **19**:1839–1841.
5. Cao QL, Zhang YP, Howard RM, Walters WM, Tsoulfas P, Whittemore SR: **Pluripotent stem cells engrafted into the normal or lesioned adult rat spinal cord are restricted to a glial lineage.** *Exp Neurol* 2001, **167**:48–58.
6. Abematsu M, Tsujimura K, Yamano M, Saito M, Kohno K, Kohyama J, Namihira M, Komiya S, Nakashima K: **Neurons derived from transplanted neural stem cells restore disrupted neuronal circuitry in a mouse model of spinal cord injury.** *J Clin Invest* 2010, **120**:3255–3266.
7. Iwanami A, Kaneko S, Nakamura M, Kanemura Y, Mori H, Kobayashi S, Yamasaki M, Momoshima S, Ishii H, Ando K, Tanioka Y, Tamaoki N, Nomura T, Toyama Y, Okano H: **Transplantation of human neural stem cells for spinal cord injury in primates.** *J Neurosci Res* 2005, **80**:182–190.
8. Salazar DL, Uchida N, Hamers FPT, Cummings BJ, Anderson AJ: **Human Neural Stem Cells Differentiate and promote locomotor recovery in an early chronic spinal cord injury NOD-scid mouse model.** *PLoS One* 2010, **5**:e12272.
9. Parr AM, Kulbatski I, Tator CH: **Transplantation of adult rat spinal cord stem/progenitor cells for spinal cord injury.** *J Neurotrauma* 2007, **24**:835–845.
10. Kusano K, Enomoto M, Hirai T, Tsoulfas P, Sotome S, Shinomiya K, Okawa A: **Transplanted neural progenitor cells expressing mutant NT3 promote myelination and partial hindlimb recovery in the chronic phase after spinal cord injury.** *Biochem Biophys Res Commun* 2010, **393**:812–817.
11. Cusimano M, Biziato D, Brambilla E, Donega M, Alfaro-Cervello C, Snider S, Salani G, Pucci F, Comi G, Garcia-Verdugo JM, De Palma M, Martino G, Pluchino S: **Transplanted neural stem/precursor cells instruct phagocytes and reduce secondary tissue damage in the injured spinal cord.** *Brain* 2012, **135**:447–460.
12. Karimi-Abdolrezaee S, Eftekharpour E, Wang J, Morshead CM, Fehlings MG: **Delayed transplantation of adult neural precursor cells promotes remyelination and functional neurological recovery after spinal cord injury.** *J Neurosci* 2006, **26**:3377–3389.
13. Contag CH, Bachmann MH: **Advances in in vivo bioluminescence imaging of gene expression.** *Annu Rev Biomed Eng* 2002, **4**:235–260.
14. Hara-Miyauchi C, Tsuji O, Hanyu A, Okada S, Yasuda A, Fukano T, Akazawa C, Nakamura M, Imamura T, Matsuzaki Y, Okano HJ, Miyawaki A, Okano H: **Bioluminescent system for dynamic imaging of cell and animal behavior.** *Biochem Biophys Res Commun* 2012, **419**:188–193.
15. Kanemura Y, Mori H, Kobayashi S, Islam O, Kodama E, Yamamoto A, Nakanishi Y, Arita N, Yamasaki M, Okano H, Hara M, Miyake J: **Evaluation of in vitro proliferative activity of human fetal neural stem/progenitor cells using indirect measurements of viable cells based on cellular metabolic activity.** *J Neurosci Res* 2002, **69**:869–879.
16. Takahashi Y, Tsuji O, Kumagai G, Hara CM, Okano HJ, Miyawaki A, Toyama Y, Okano H, Nakamura M: **Comparative study of methods for administering neural stem/progenitor cells to treat spinal cord injury in mice.** *Cell Transplant* 2011, **20**:727–739.

17. Yasuda A, Tsuji O, Shibata S, Nori S, Takano M, Kobayashi Y, Takahashi Y, Fujiyoshi K, Hara CM, Miyawaki A, Okano HJ, Toyama Y, Nakamura M, Okano H: **Significance of remyelination by neural stem/progenitor cells transplanted into the injured spinal cord.** *Stem Cells* 2011, **29**:1983–1994.
18. Anderson AJ, Haus DL, Hooshmand MJ, Perez H, Sontag CJ, Cummings BJ: **Achieving stable human stem cell engraftment and survival in the CNS: is the future of regenerative medicine immunodeficient?** *Regen med* 2011, **6**:367–406.
19. Kumamaru H, Ohkawa Y, Saiwai H, Yamada H, Kubota K, Kobayakawa K, Akashi K, Okano H, Iwamoto Y, Okada S: **Direct isolation and RNA-seq reveal environment-dependent properties of engrafted neural stem/progenitor cells.** *Nat Commun* 2012, **3**:1140.
20. Nakamura M, Houghtling RA, MacArthur L, Bayer BM, Bregman BS: **Differences in cytokine gene expression profile between acute and secondary injury in adult rat spinal cord.** *Exp Neurol* 2003, **184**:313–325.
21. Kumamaru H, Saiwai H, Ohkawa Y, Yamada H, Iwamoto Y, Okada S: **Age-related differences in cellular and molecular profiles of inflammatory responses after spinal cord injury.** *J Cell Physiol* 2012, **227**:1335–1346.
22. Kumar S, Kahn MA, Dinh L, de Vellis J: **NT-3-mediated TrkC receptor activation promotes proliferation and cell survival of rodent progenitor oligodendrocyte cells in vitro and in vivo.** *J Neurosci Res* 1998, **54**:754–765.
23. Kokuzawa J, Yoshimura S, Kitajima H, Shinoda J, Kaku Y, Iwama T, Morishita R, Shimazaki T, Okano H, Kunisada T, Sakai N: **Hepatocyte growth factor promotes proliferation and neuronal differentiation of neural stem cells from mouse embryos.** *Mol Cell Neurosci* 2003, **24**:190–197.
24. Erlandsson A, Enarsson M, Forsberg-Nilsson K: **Immature neurons from CNS stem cells proliferate in response to platelet-derived growth factor.** *J Neurosci* 2001, **21**:3483–3491.
25. Johe KK, Hazel TG, Muller T, Dugich-Djordjevic MM, McKay RD: **Single factors direct the differentiation of stem cells from the fetal and adult central nervous system.** *Genes Dev* 1996, **10**:3129–3140.
26. Nori S, Okada Y, Yasuda A, Tsuji O, Takahashi Y, Kobayashi Y, Fujiyoshi K, Koike M, Uchiyama Y, Ikeda E, Toyama Y, Yamanaka S, Nakamura M, Okano H: **Grafted human-induced pluripotent stem-cell-derived neurospheres promote motor functional recovery after spinal cord injury in mice.** *Proc Natl Acad Sci USA* 2011, **108**:16825–16830.
27. Kitamura K, Iwanami A, Nakamura M, Yamane J, Watanabe K, Suzuki Y, Miyazawa D, Shibata S, Funakoshi H, Miyatake S, Coffin RS, Nakamura T, Toyama Y, Okano H: **Hepatocyte growth factor promotes endogenous repair and functional recovery after spinal cord injury.** *J Neurosci Res* 2007, **85**:2332–2342.
28. Hawryluk GW, Mothe A, Wang J, Wang S, Tator C, Fehlings MG: **An in vivo characterization of trophic factor production following neural precursor cell or bone marrow stromal cell transplantation for spinal cord injury.** *Stem Cell Dev* 2012, **21**:2222–2238.
29. Tuszynski MH, Gabriel K, Gage FH, Suhr S, Meyer S, Rosetti A: **Nerve growth factor delivery by gene transfer induces differential outgrowth of sensory, motor, and noradrenergic neurites after adult spinal cord injury.** *Exp Neurol* 1996, **137**:157–173.
30. Kumagai G, Okada Y, Yamane J, Nagoshi N, Kitamura K, Mukaino M, Tsuji O, Fujiyoshi K, Katoh H, Okada S, Shibata S, Matsuzaki Y, Toh S, Toyama Y, Nakamura M, Okano H: **Roles of ES cell-derived gliogenic neural stem/progenitor cells in functional recovery after spinal cord injury.** *PLoS One* 2009, **4**:e7706.
31. Bregman BS: **Spinal cord transplants permit the growth of serotonergic axons across the site of neonatal spinal cord transection.** *Brain Res* 1987, **431**:265–279.
32. Saruhashi Y, Young W, Perkins R: **The recovery of 5-HT immunoreactivity in lumbosacral spinal cord and locomotor function after thoracic hemisection.** *Exp Neurol* 1996, **139**:203–213.
33. Predy R, Malhotra SK: **Reactive astrocytes in lesioned rat spinal cord: effect of neural transplants.** *Brain Res Bull* 1989, **22**:81–87.
34. Grijalva I, Guizar-Sahagun G, Salgado-Ceballos H, Ibarra A, Franco-Bourland R, Espitia L, Madrazo I: **Improvement of host-graft adhesion by enzymatic manipulation of the subacute spinal cord contusion area in the rat.** *Transplant Proc* 1996, **28**:3340–3342.
35. Beck KD, Nguyen HX, Galvan MD, Salazar DL, Woodruff TM, Anderson AJ: **Quantitative analysis of cellular inflammation after traumatic spinal cord injury: evidence for a multiphasic inflammatory response in the acute to chronic environment.** *Brain* 2010, **133**:433–447.
36. Popovich PG, Wei P, Stokes BT: **Cellular inflammatory response after spinal cord injury in Sprague–Dawley and Lewis rats.** *J Comp Neurol* 1997, **377**:443–464.
37. Kigerl KA, Gensel JC, Ankeny DP, Alexander JK, Donnelly DJ, Popovich PG: **Identification of Two Distinct Macrophage Subsets with Divergent Effects Causing either Neurotoxicity or Regeneration in the Injured Mouse Spinal Cord.** *J Neurosci* 2009, **29**:13435–13444.
38. Block ML, Zecca L, Hong JS: **Microglia-mediated neurotoxicity: uncovering the molecular mechanisms.** *Nat Rev Neurosci* 2007, **8**:57–69.
39. Busch SA, Hamilton JA, Horn KP, Cuascut FX, Cutrone R, Lehman N, Deans RJ, Ting AE, Mays RW, Silver J: **Multipotent adult progenitor cells prevent macrophage-mediated axonal dieback and promote regrowth after spinal cord injury.** *J Neurosci* 2011, **31**:944–953.
40. Mukaino M, Nakamura M, Yamada O, Okada S, Morikawa S, Renault-Mihara F, Iwanami A, Ikegami T, Ohsugi Y, Tsuji O, Katoh H, Matsuzaki Y, Toyama Y, Liu M, Okano H: **Anti-IL-6-receptor antibody promotes repair of spinal cord injury by inducing microglia-dominant inflammation.** *Exp Neurol* 2010, **224**:403–414.
41. Schilling M, Besselmann M, Muller M, Strecker JK, Ringelstein EB, Kiefer R: **Predominant phagocytic activity of resident microglia over hematogenous macrophages following transient focal cerebral ischemia: an investigation using green fluorescent protein transgenic bone marrow chimeric mice.** *Exp Neurol* 2005, **196**:290–297.
42. Mantovani A, Sozzani S, Locati M, Allavena P, Sica A: **Macrophage polarization: tumor-associated macrophages as a paradigm for polarized M2 mononuclear phagocytes.** *Trends Immunol* 2002, **23**:549–555.
43. Busch SA, Horn KP, Silver DJ, Silver J: **Overcoming macrophage-mediated axonal dieback following CNS injury.** *J Neurosci* 2009, **29**:9967–9976.
44. Kokaia Z, Martino G, Schwartz M, Lindvall O: **Cross-talk between neural stem cells and immune cells: the key to better brain repair?** *Nat Neurosci* 2012, **15**:1078–1087.
45. Ziv Y, Avidan H, Pluchino S, Martino G, Schwartz M: **Synergy between immune cells and adult neural stem/progenitor cells promotes functional recovery from spinal cord injury.** *Proc Natl Acad Sci USA* 2006, **103**:13174–13179.
46. Andrews T, Zhang P, Bhat NR: **TNFalpha potentiates IFNgamma-induced cell death in oligodendrocyte progenitors.** *J Neurosci Res* 1998, **54**:574–583.
47. Ben-Hur T, Ben-Menachem O, Furer V, Einstein O, Mizrachi-Kol R, Grigoriadis N: **Effects of proinflammatory cytokines on the growth, fate, and motility of multipotential neural precursor cells.** *Mol Cell Neurosci* 2003, **24**:623–631.
48. Silver J, Miller JH: **Regeneration beyond the glial scar.** *Nat Rev Neurosci* 2004, **5**:146–156.
49. Ikegami T, Nakamura M, Yamane J, Katoh H, Okada S, Iwanami A, Watanabe K, Ishii K, Kato F, Fujita H, Takahashi T, Okano HJ, Toyama Y, Okano H: **Chondroitinase ABC combined with neural stem/progenitor cell transplantation enhances graft cell migration and outgrowth of growth-associated protein-43-positive fibers after rat spinal cord injury.** *Eur J Neurosci* 2005, **22**:3036–3046.
50. Bradbury EJ, Moon LD, Popat RJ, King VR, Bennett GS, Patel PN, Fawcett JW, McMahon SB: **Chondroitinase ABC promotes functional recovery after spinal cord injury.** *Nature* 2002, **416**:636–640.
51. Karimi-Abdolrezaee S, Eftekharpour E, Wang J, Schut D, Fehlings MG: **Synergistic Effects of Transplanted Adult Neural Stem/Progenitor Cells, Chondroitinase, and Growth Factors Promote Functional Repair and Plasticity of the Chronically Injured Spinal Cord.** *J Neurosci* 2010, **30**:1657–1676.
52. Reynolds BA, Tetzlaff W, Weiss S: **A multipotent EGF-responsive striatal embryonic progenitor cell produces neurons and astrocytes.** *J Neurosci* 1992, **12**:4565–4574.
53. Nagai T, Ibata K, Park ES, Kubota M, Mikoshiba K, Miyawaki A: **A variant of yellow fluorescent protein with fast and efficient maturation for cell-biological applications.** *Nat Biotechnol* 2002, **20**:87–90.
54. Yamane J, Nakamura M, Iwanami A, Sakaguchi M, Katoh H, Yamada M, Momoshima S, Miyao S, Ishii K, Tamaoki N, Nomura T, Okano HJ, Kanemura Y, Toyama Y, Okano H: **Transplantation of galectin-1-expressing human neural stem cells into the injured spinal cord of adult common marmosets.** *J Neurosci Res* 2010, **88**:1394–1405.
55. Lockhart DJ, Dong H, Byrne MC, Follettie MT, Gallo MV, Chee MS, Mittmann M, Wang C, Kobayashi M, Horton H, Brown EL: **Expression monitoring by hybridization to high-density oligonucleotide arrays.** *Nat Biotechnol* 1996, **14**:1675–1680.

56. Heishi M, Ichihara J, Teramoto R, Itakura Y, Hayashi K, Ishikawa H, Gomi H, Sakai J, Kanaoka M, Taiji M, Kimura T: **Global gene expression analysis in liver of obese diabetic db/db mice treated with metformin.** *Diabetologia* 2006, **49**:1647–1655.
57. Tsuji O, Miura K, Okada Y, Fujiyoshi K, Mukaino M, Nagoshi N, Kitamura K, Kumagai G, Nishino M, Tomisato S, Higashi H, Nagai T, Katoh H, Kohda K, Matsuzaki Y, Yuzaki M, Ikeda E, Toyama Y, Nakamura M, Yamanaka S, Okano H: **Therapeutic potential of appropriately evaluated safe-induced pluripotent stem cells for spinal cord injury.** *Proc Natl Acad Sci USA* 2010, **107**:12704–12709.
58. Basso DM, Fisher LC, Anderson AJ, Jakeman LB, McTigue DM, Popovich PG: **Basso Mouse Scale for locomotion detects differences in recovery after spinal cord injury in five common mouse strains.** *J Neurotraum* 2006, **23**:635–659.
59. Ogura H, Matsumoto M, Mikoshiba K: **Motor discoordination in mutant mice heterozygous for the type 1 inositol 1,4,5-trisphosphate receptor.** *Behav Brain Res* 2001, **122**:215–219.
60. Springer JE, Rao RR, Lim HR, Cho SI, Moon GJ, Lee HY, Park EJ, Noh JS, Gwag BJ: **The functional and neuroprotective actions of Neu 2000, a dual-acting pharmacological agent, in the treatment of acute spinal cord injury.** *J Neurotraum* 2010, **27**:139–149.

doi:10.1186/1756-6606-6-3
Cite this article as: Nishimura *et al.*: Time-dependent changes in the microenvironment of injured spinal cord affects the therapeutic potential of neural stem cell transplantation for spinal cord injury. *Molecular Brain* 2013 **6**:3.

Spine
BASIC SCIENCE

SPINE Volume 38, Number 2, pp E66–E72

In Vivo Tracing of Neural Tracts in Tiptoe Walking Yoshimura Mice by Diffusion Tensor Tractography

Morito Takano, MD,*† Yuji Komaki, MS,†‡ Keigo Hikishima, PhD,†‡ Tsunehiko Konomi, MD,*†
Kanehiro Fujiyoshi, MD, PhD,§ Osahiko Tsuji, MD, PhD,* Yoshiaki Toyama, MD, PhD,*
Hideyuki Okano, MD, PhD,† and Masaya Nakamura, MD, PhD*

Study Design. Basic imaging experiment.

Objective. To determine whether *in vivo* diffusion tensor tractography (DTT) can be used to evaluate the axonal disruption of the chronically compressed spinal cord in tiptoe walking Yoshimura (*twy*) mice.

Summary of Background Data. In cervical ossification of the posterior longitudinal ligament, axonal disruption results in motor and sensory functional impairment. *Twy* mice develop spontaneous calcification in the cervical ligaments, which causes chronic compression of the spinal cord. DTT is emerging as a powerful tool for tracing axonal fibers *in vivo*.

Methods. Five *twy* mice were subjected to DTT at 6, 15, and 20 weeks of age. Magnetic resonance imaging was performed using a 7.0-Tesla magnet (Biospec 70/16; Billerica, MA) with a CryoProbe. Diffusion tensor images were analyzed using TrackVis (Massachusetts General Hospital, MA). Motor performance was evaluated by Rotarod treadmill test and Digigait analysis. Histological analysis was performed by hematoxylin-eosin staining and immunostaining for RT-97 and SMI-31.

Results. High resolution DTT of *twy* mice *in vivo* was successful. A lower number of RT-97- or SMI-31–positive fibers were associated with more severe spinal cord compression, which was determined by observing the ligamentous calcification at the C2–C3 level in each *twy* mouse. The severity of canal stenosis based on magnetic resonance images was strongly correlated with the axial area of the spinal cord. The tract fiber (TF) ratio (the number of TFs at the C2–C3 level/the number of TFs at the C0–C1 level) was strongly correlated with the RT-97/SMI-31–positive area and with motor function (rotarod latency, stride length). Furthermore, a two-part linear regression analysis showed that canal stenosis around 50% to 60% caused a sharp decrease in the TF ratio before the deterioration of motor function.

Conclusion. We conclude that DTT could be useful for detecting the early changes associated with the compressed spinal cord in cervical ossification of the posterior longitudinal ligament.

Key words: diffusion tensor tractography, *twy* mouse, ossification of the posterior longitudinal ligament. **Spine 2013;38:E66–E72**

Ossification of the posterior longitudinal ligament (OPLL) of the cervical spine compresses the spinal cord and causes myelopathy. Surgical treatment for OPLL is clearly indicated when the patient shows severe or progressive cervical myelopathy, and the surgery should be performed as soon as possible. However, for patients without any symptoms or with only mild myelopathy despite of evident OPLL on plain radiograph of the cervical spine, the indication for and timing of surgical treatment remain controversial. Although conventional magnetic resonance imaging (MRI) provides useful information about the compressed spinal cord,[1–3] a discrepancy is sometimes seen between the degree of spinal cord compression and the clinical symptoms.

Diffusion tensor imaging (DTI) is an MRI technique that evaluates the diffusion of extracellular water molecules within white matter fibers. The DTI parameters are described as disclosing subtle pathological changes in white matter integrity, and they have been useful for analyzing various central nervous system disorders.[4–8] Diffusion tensor tractography (DTT) refers to the analysis and reconstruction of the DTI data, by which the orientation of nerve fibers can be followed to trace specific neural pathways.[9] The applications of DTT were recently reported to include cases of spinal cord compression in humans.[10–12] DTT is useful for grading the neurological severity in cervical spondylotic myelopathy because it provides objective measures in terms of microstrucural changes. However, to the best of our knowledge, there are no reports on the chronological changes in this disease, including comparisons between

From the *Department of Orthopaedic Surgery, Keio University, Tokyo, Japan; †Department of Physiology, Keio University, Tokyo, Japan; ‡Central Institute for Experimental Animals, Kanagawa, Japan; and §National Hospital Organization Murayama Medical Center, Tokyo, Japan.

Acknowledgment date: April 12, 2012. First revision date: July 3, 2012. Second revision date: October 18, 2012. Acceptance date: October 19, 2012.

The device(s)/drug(s) is/are FDA-approved or approved by corresponding national agency for this indication.

Ministry of Health, Labor and Welfare Sciences Research Grant funds were received to support this work.

No relevant financial activities outside the submitted work.

Address correspondence and reprint requests to Masaya Nakamura, MD, PhD, Department of Orthopaedic Surgery, Keio University, Shinanomachi 35, Shinjuku-Ku, Tokyo, 160-8582, Japan; E-mail: masa@a8.keio.jp

DOI: 10.1097/BRS.0b013e31827aacc2

DTT findings and histological/functional analyses in animal models.

Tiptoe walking Yoshimura (*twy*) mice are reported to be a good *in vivo* model for the pathological changes underlying spinal cord dysfunction related to chronic compression.[13–15] *Twy* mice develop progressive spinal cord dysfunction secondary to extradural calcified deposits at C2–C3 that cause cervical cord compression. This mouse develops spontaneous spinal cord compression, so it is suitable for investigating the effects of chronic mechanical compression of the spinal cord without any artificial manipulation. Although Yu *et al*[16] showed the postmortem T2-weighted MRI of sagittal sections derived from *twy* mice using 3T MRI, the sequential changes of *in vivo* MRI in the *twy* mouse have not been fully elucidated. The purpose of the present study is to determine the relevance of DTT for evaluating the tract fibers (TFs) of the compressed spinal cord by comparing the chronological *in vivo* DTT findings with histological findings and motor performance in *twy* mice.

MATERIALS AND METHODS

Animal Model

Ten *twy* mice were obtained from a breeding colony of the Central Institute for Experimental Animals (Kawasaki, Japan). Mutant *twy* mice were maintained by brother-sister matings of heterozygotes at the Central Research Institute.[16,17] *Twy* mice harbor an autosomal recessive mutation in the nucleotide pyrophosphatase (*NPPS*) gene.[15] *Twy* mice were housed in groups under a 12-hour light/dark cycle, with access to food and water *ad libitum*. All experiments were performed in accordance with the Guidelines for the Care and Use of Laboratory Animals of Keio University School of Medicine and Central Institute for Experimental Animals.

Magnetic Resonance Imaging

MRI was chronologically performed at 6, 15, and 20 weeks of age using a 7.0-Tesla magnet (BioSpec 70/16; Bruker BioSpin, Ettlingen, Germany) with a cryogenic quadrature RF surface probe (CryoProbe; Bruker BioSpin AG, Fällanden, Switzerland) to improve the sensitivity.[18,19] Conventional and diffusion tensor MRI were performed under general anesthesia induced by intramuscular injection of ketamine (50 mg/kg; Sankyo, Tokyo, Japan) and xylazine (5 mg/kg; Bayer, Leverkusen, Germany) and maintained by isoflurane (Foren; Abbott, Tokyo, Japan). The animal's pulse, arterial oxygen saturation, and rectal temperature were monitored during the MRI. DTI data sets were acquired with a spin-echo sequence based on the Stejskal-Tanner diffusion preparation. The scanning parameters were as follows: saggital T1-weighted images (RARE, eTE/TR: 10.5 ms/800 ms), saggital T2-weighted images (T2WI) (RARE, eTE/TR: 37.5/2000 ms), axial T2WIs (RARE, eTE/TR: 21.5 ms/1200 ms), diffusion tensor images (SE-DTI, TE/TR: 22.3 ms/2750 ms).

Diffusion Tensor Analysis

Diffusion tensor tractographic images were computed using the Diffusion Toolkit and TrackVis software (Massachusetts General Hospital, MA). The diffusion tensor can be represented as an ellipsoid, where a proton at the center of the voxel has an equal probability of diffusing to any point in that ellipsoid. Fiber tracking was initiated from a manually selected region of interest (ROI), from which tracking lines were propagated bidirectionally according to the principal eigenvector in each voxel. For the tractography, an ROI was placed at the C2–C3 level as the epicenter ROI and at the C0–C1 level as the control ROI. We determined the number of TFs in each specimen at the C2–C3 level (epicenter site) and the C0–C1 level (control/rostral site). The tracking parameters were as follows: angle threshold, 35°; minimum length threshold, 1.5 mm; rendering with tube mode (radius = 0.003, number of sides = 5); color code scale for

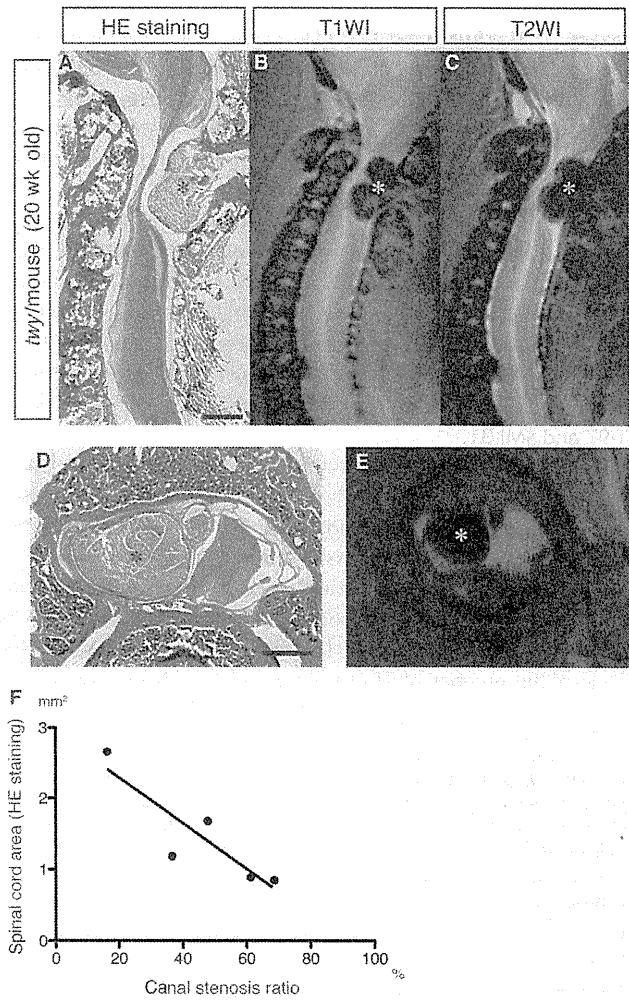

Figure 1. Representative HE-stained sagittal and axial images of the *twy* mice. (**A**) Scale bar: 1 mm, (**D**) 500 μm. (**B, C, E**) Sagittal and axial MRI showed notable cervical spinal cord compression resulting from ectopic calcification (*). (**F**) The spinal cord area was correlated with the canal stenosis ratio (r = −0.7840). HE indicates hematoxylin-eosin MRI, magnetic resonance imaging; *twy* tiptoe walking Yoshimura.

TABLE 1. Definition of the Canal Stenosis Ratio and Tract Fiber (TF) Ratio

Canal stenosis ratio = 100 − (spinal cord area/spinal canal area) × 100 TF ratio = number of tract fibers at the C2–C3 level/number of tract fibers at the C0–C1 level

fractional anisotropy (red indicates high anisotropy; blue, low anisotropy).

Behavioral Analyses

The motor function of 20-week-old *twy* mice was evaluated using a Rotarod treadmill apparatus (Muromachi Kikai Co., Ltd., Tokyo, Japan) and the DigiGait Image Analysis System (Mouse Specifics, Quincy, MA). In the Rotarod treadmill test, each *twy* mouse was tested by monitoring the time (latency) that the animal spent on the rod as it rotated at 10 rpm, in a 2-minute session.[20] Three trials were conducted, and the average number of seconds was recorded. In the footprint analysis using the Digigait system, the stride length was measured as long as the *twy* mouse could walk with consistent weight-supported forelimb steps, on the treadmill set at a speed of 8 cm/s.

Histological Analysis

After the behavioral analyses, the *twy* mice were anesthetized and transcardially perfused with 4% paraformaldehyde in 0.1 M PBS. The spinal cord and spinal canal were removed and immersed in Decalcifying Solution B (Dako, Glostrup, Denmark) for 3 days. These samples were then embedded in optimal cutting temperature compound (Sakura Finetechnical Co., Ltd., Tokyo, Japan) and sectioned in the sagittal/axial plane at 20 μm on a cryostat (Leica CM3050 S, Wetzlar, Germany). The spinal cords and spinal canals were histologically evaluated by hematoxylin-eosin (HE) staining and immunohistochemistry. The tissue sections were stained with the following primary antibodies: anti-RT-97 (mouse IgG_1, 1:200; Millipore, MA) for normal neurofilaments, and anti-SMI-31 (mouse IgG_1, 1:200; Covance, Princeton, NJ) for hyperphosphorylated normal axons. A biotinylated secondary antibody (Jackson Immunoresearch Laboratory, Inc., West Grove, PA) was used after exposing the sections to 0.3% H_2O_2 for 30 minutes at room temperature to inactivate endogenous peroxidase. The signals were enhanced with the Vectastain ABC kit (Vector Laboratories, Inc., CA). The samples were examined with an inverted fluorescence microscope (BZ 9000; Keyence Co., Osaka, Japan). To quantify the HE-stained and immunostained sections, images obtained with the BZ9000 microscope were quantified by Keyence Analysis Software (Keyence Co., Woodcliff Lake, NJ). Constant threshold values were maintained for all the analyses. HE-stained images were taken at C2–C3 (the lesion epicenter) in axial sections at ×20 magnification to measure the transverse area of the spinal cord. The RT-97- and SMI-31–stained images were automatically captured at the lesion epicenter in axial sections at ×100 magnification, and the RT-97- and SMI-31–positive areas of the whole spinal cord were quantified.

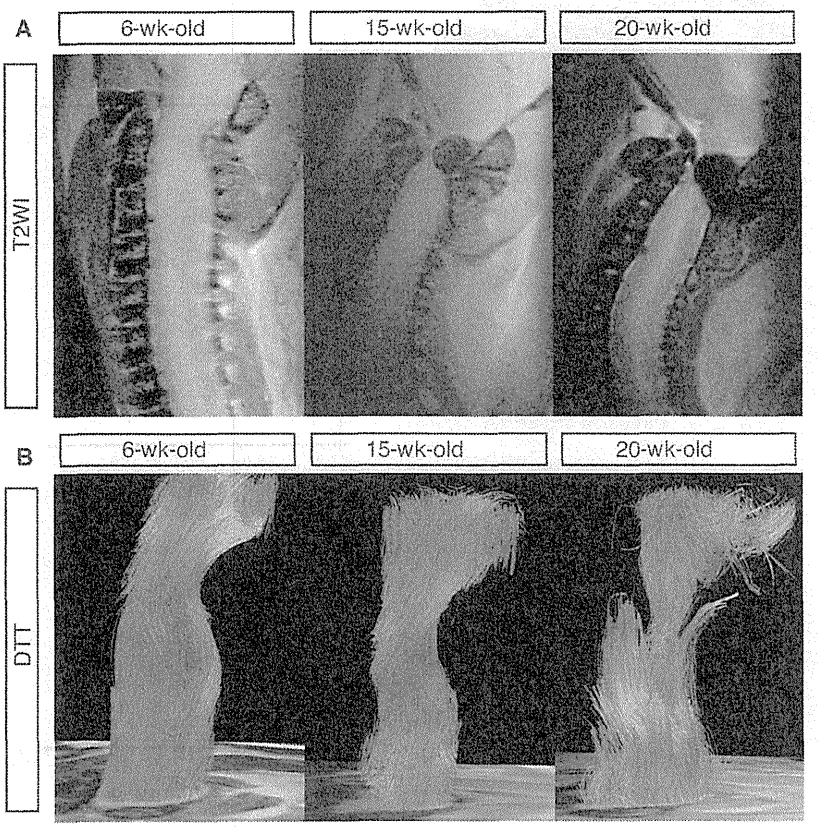

Figure 2. (A) Sagittal T2-weighted image and (B) diffusion tensor tractography of the *twy* mice observed chronologically (at 6, 15, and 20 weeks of age). The results showed that calcification in the atlanto-axial membrane gradually progressed, whereas the number of tract fibers gradually decreased. *twy* indicates tiptoe walking Yoshimura.

Statistical Analysis

All values are presented as the mean ± standard error of the mean. Pearson correlation coefficients were calculated to determine the correlations among the spinal canal stenosis rates, the TF parameters, and the histological/functional parameters. A two-part linear regression analysis was performed as described previously.[21] The GraphPad Prism software (version 5.0d) was used for the analyses (GraphPad Software, Inc., La Jolla, CA).

RESULTS

Comparisons of MR Images With Histology

The conventional and diffusion tensor MRI were completed in 5 out of 10 *twy* mice until they were 20 weeks old. In 20-week-old *twy* mice, severe spinal cord compression was observed at the C2–C3 level due to calcification of the atlanto-axial membrane (Figure 1A). Consistent with the histological findings, the MR images precisely depicted severe spinal cord compression (Figures 1B, C). To examine the effect of ectopic calcification on the spinal cord in 20-week-old *twy* mice, we measured the transverse area of the spinal cord histologically and compared it with the canal stenosis ratio (Table 1) (Figures 1D, E). There was a significant negative correlation between the transverse area of the spinal cord and the canal stenosis ratio ($r = -0.7840$, $P = 0.0457$, Figure 1F).

Sequential Changes in Diffusion Tensor Tractography

Chronological T2WI of the upper cervical spinal cord enabled the progression of spinal cord compression due to ectopic calcification to be depicted in the same *twy* mouse (Figure 2A). Mild and moderate spinal cord compression caused the TFs to detour around the ectopic calcification at 6 and 15 weeks of age, whereas the TFs were interrupted by severe spinal cord compression at 20 weeks of age (Figure 2B). To analyze the sequential changes in the TFs of the compressed spinal cords quantitatively, we determined the canal stenosis ratios and configured TF ratios (Figure 3A, Table 1) in 6-, 15-, and 20-week-old *twy* mice. The TF ratio did not significantly change in the 15-week-olds, but decreased sharply in the 20-week-olds (Figure 3B). To examine the significance of the depicted TFs, we compared the TFs depicted by DTT

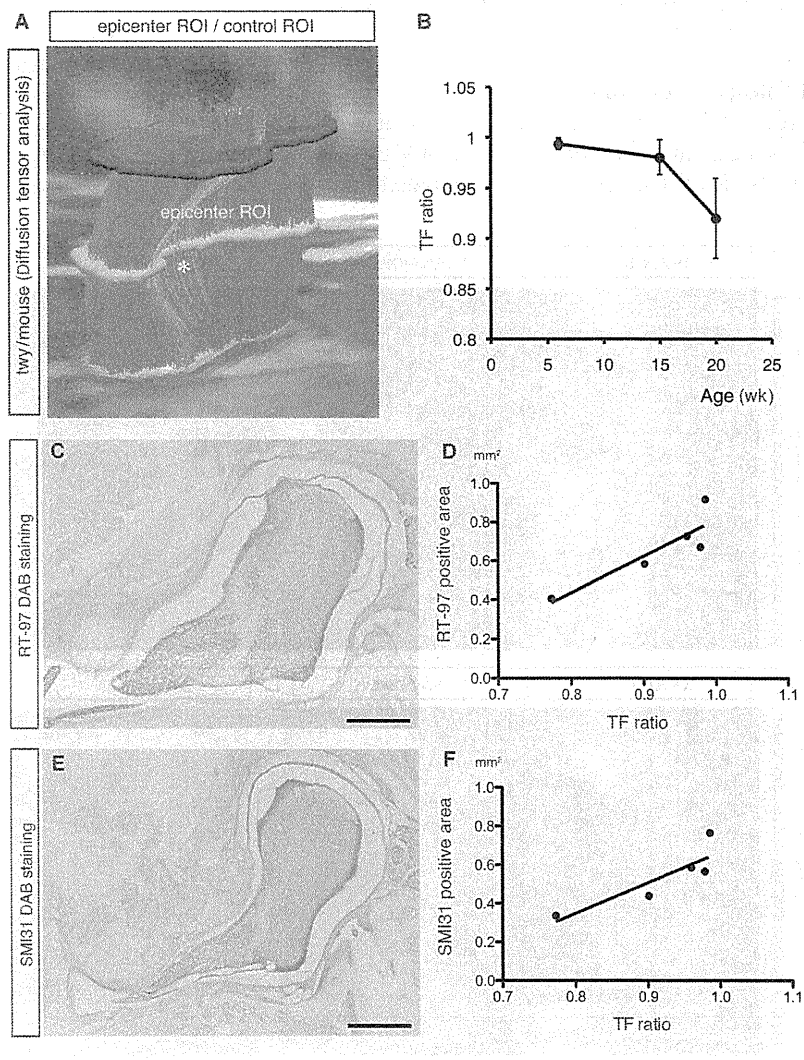

Figure 3. (A) The tract fibers were generated by placing the ROIs at the C0–C1 and C2–C3 levels. (B) The TF ratio tended to decrease with the animal's age. Correlations between the TF ratio and the area of neurofilament staining for RT-97 (C, D: $r = 0.7865$) and SMI-31 (E, F: $r = 0.7746$). Scale bar: 500 μm. TF indicates tract fiber; ROI, region of interest.

with the RT-97- and SMI-31–positive fibers in the 20-week-old *twy* mice (Figures 3C, E). There was a positive correlation between the TF ratio and the RT-97–positive area ($r = 0.7865$, $P = 0.0449$, Figure 3D) and SMI-31–positive area ($r = 0.7746$, $P = 0.0489$, Figure 3F).

Correlations Among the TF Ratio, Canal Stenosis Rate, and Motor Performance

The canal stenosis progressed with the age of the *twy* mice. To examine the chronological relationship between the TF ratio and canal stenosis ratio, we analyzed their correlation in 5 *twy* mice at 6, 15, and 20 weeks of age (Figure 4A). As the *twy* mice became older, the canal stenosis became more prominent, causing a decrease in the TF ratio. Interestingly, a two-part linear regression analysis revealed that canal stenosis around 50% to 60% caused a sharp decrease in the TF ratio (intersection point: 52%, Figure 4B).

Because *twy* mice show progressive paralysis due to the chronic spinal cord compresion,[22] we examined the motor function in the mice by the Rotarod treadmill test and Digigait analysis, and compared the results with the TF ratio and canal stenosis ratio in the 20-week-old *twy* mice. Both the Rotarod treadmill latency and stride length sharply decreased when the TF ratio was below 0.9 (Figures 5A, B) and canal stenosis ratio was more than 60% (Figures 5C, D). Consistent with the Rotarod treadmill analysis, the Digigait analysis revealed that 2 *twy* mice with severe spinal cord compression (canal stenosis ratio >60%) could not walk on the treadmill, whereas the other *twy* mice with mild or moderate spinal cord compression (canal stenosis ratio <50%) could walk on the treadmill at a speed of 8 cm/s.

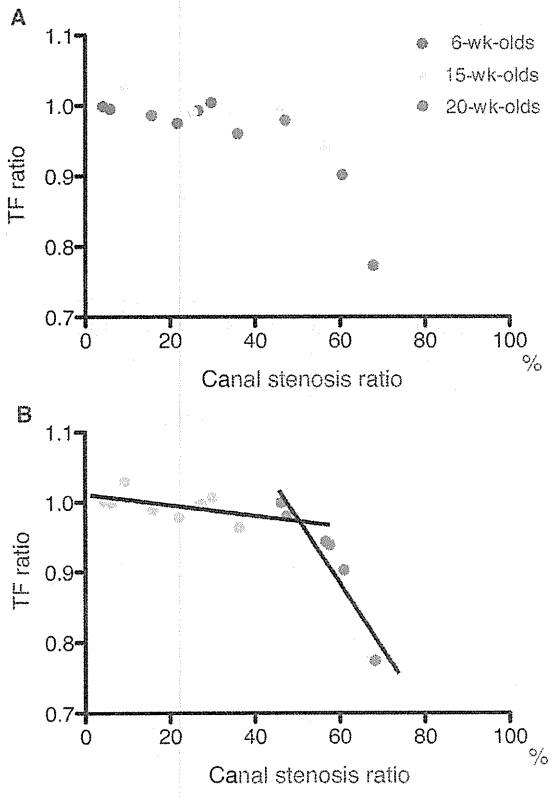

Figure 4. (A) Correlations between the TF ratio and canal stenosis ratio (blue dots: 6 week-olds, yellow dots: 15 week-olds, red dots: 20 week-olds). (B) Two-part linear regression analysis showed that canal stenosis around 50% to 60% caused a sharp decrease in the TF ratio (light green: $r = -0.2827$, dark green: $r = -0.8705$). TF indicates tract fiber.

DISCUSSION

In the present study, we show that *in vivo* DTT could depict the chronological changes in the TFs of the chronic progressive spinal cord compression in *twy* mice. The number of TFs depicted by DTT was significantly correlated with the areas of RT-97$^+$ and SMI-31$^+$ neurofilaments and the results of motor function analyses. In addition, our results suggest that, in particular, around 50% to 60% spinal canal stenosis causes a sharp decrease in the TFs even before a prominent neurological deficit is seen.

Previous studies on the surgical outcomes of patients with OPLL demonstrated that the postoperative recovery is poor in those with a greater than 50% to 60% compromise of the spinal canal by the ossified lesion.[23,24] Recent reports examining the surgical option for treating patients with cervical myelopathy caused by OPLL[25–27] suggested that the surgical results depend on the severity of the preoperative neurological deficit, and, therefore, the cervical myelopathy must be diagnosed as early as possible. However, there are no reports describing a useful and objective tool for determining the surgical indication for cervical myelopathy. Conventional MRI undoubtedly provides useful information about the compressed spinal cord. However, sometimes there is a discrepancy between the degree of spinal cord compression and the clinical symptoms.

We previously demonstrated that DTT is very useful for examining spinal cord injuries and peripheral nerve injuries in experimental animal models.[28,29] Fujiyoshi *et al*[28] reported that DTT is effective for visualizing both intact and surgically disrupted long spinal tracts in adult common marmosets. Takagi *et al*[29] also reported that DTT can be used to evaluate Wallerian degeneration and the regeneration of peripheral nerves after injury. In the clinic, Kara *et al*[12] suggested that DTT can show abnormalities in the compressive spinal cord before the development of T2 hyperintensity on conventional MRI sequences in patients with cervical spondylotic myelopathy. Mamata *et al*[30] also reported that 54% patients with cervical spondylosis without any abnormal signals on T2WIs showed abnormalities in the fractional anisotropy and apparent diffusion coefficient values at the level of spinal cord stenosis. Although DTT is thought to have great potential for detecting cervical myelopathy, it is unclear how DTT would show the pathological changes of the compressed spinal cord. Accordingly, we focused on *twy* mice, which develop spontaneous cervical myelopathy due to ectopic ossified ligaments.

Baba *et al*[31] previously reported that the chronic compression of the cervical spinal cord of *twy* mice causes the loss of motoneurons at the injury epicenter. Yato *et al*[32] also reported that spinal motorneuron atrophy and loss in the gray matter of *twy* mice were observed when the severity of spinal canal stenosis was 30% or more. Given the variation in the severity

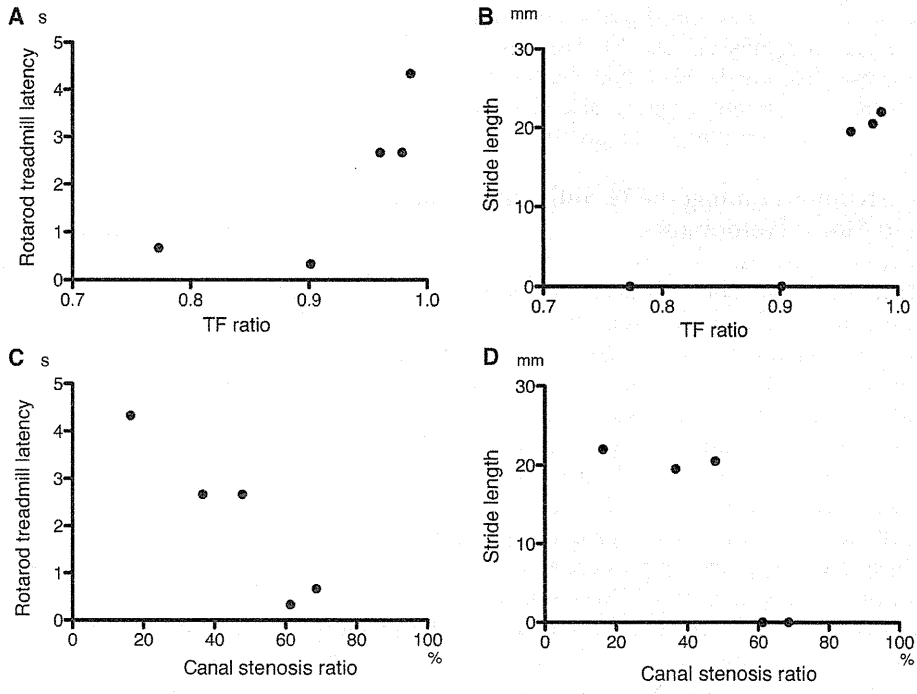

Figure 5. Correlations among the TF ratio, canal stenosis ratio, and functional parameters. (**A**) TF ratio and Rotarod treadmill latency; (**B**) TF ratio and stride length; (**C**) canal stenosis rate and Rotarod treadmill latency; and (**D**) canal stenosis rate and stride length. TF indicates tract fiber.

of spinal cord compression due to ligamentous calcification in these mice, it is important to observe the chronological changes in the spinal cord of live *twy* mice, which has never been reported previously.

In the present study, we performed *in vivo* imaging of *twy* mice with a 7T MRI and CryoProbe, and examined the chronological changes in their compressed spinal cords. To the best of our knowledge, this is the first study to show the chronological changes of DTT parameters in *twy* mice using high resolution MRI. We demonstrated that the TF ratio decreased sharply at around 50% to 60% spinal canal stenosis. Our results resemble clinical evidence and suggest that irreversible changes in neurofilaments increase dramatically at around 50% to 60% spinal canal stenosis. It is noteworthy that the decrease in TF ratio preceded the functional deterioration, which occurred at around 60% spinal canal stenosis.

There are some limitations of the present study. In *twy* mice, spinal cord compression occurs only at the C2–C3 level, which is quite rare in the clinic. Most patients experiencing OPLL have chronic spinal cord compression at multiple levels. Therefore, animal models with multilevel spinal canal stenosis should be examined in future studies. Another limitation is the small number of experimental animals in the present study. Because the general anesthesia and neck position in hyperflexion for MRI frequently caused the animal's death due to respiratory problems, the number of *twy* mice undergoing successful chronological DTT was limited. The other limitation is related to the MRI device. Because the voxel size in this study was 100×100×100 μm, the TFs depicted by DTT were not axonal fibers themselves. The range of the captured spinal cord was restricted due to the size of the Cryoprobe.

In conclusion, DTT could be a new effective imaging modality in patients with cervical myelopathy due to ligamentous calcifications. In this study, subtle damage visible in the neurofilaments could be quantitatively analyzed at each stage of disease by measuring the TFs. Thus, in a clinical setting, the TF ratio could be a useful parameter for making decisions about the indications and timing of surgical treatment for cervical myelopathy due to OPLL.

Key Points

- *In vivo* DTT of *twy* mice could detect the disruption of TFs in the chronically compressed spinal cord.
- The TF damage depicted by DTT correlated with immunostained neurofilaments and the results of motor function analyses.
- In *twy* mice, spinal canal stenosis over around 50% to 60% caused a sharp decrease in the number of TFs.

References

1. Vedantam A, Jonathan A, Rajshekhar V. Association of magnetic resonance imaging signal changes and outcome prediction after surgery for cervical spondylotic myelopathy. *J Neurosurg Spine* 2011;15:660–6.
2. Yagi M, Ninomiya K, Kihara M, et al. Long-term surgical outcome and risk factors in patients with cervical myelopathy and a change in signal intensity of intramedullary spinal cord on Magnetic Resonance imaging. *J Neurosurg Spine* 2010;12:59–65.
3. Matsuyama Y, Kawakami N, Yanase M, et al. Cervical myelopathy due to OPLL: clinical evaluation by MRI and intraoperative spinal sonography. *J Spinal Disord Tech* 2004;17:401–4.
4. Chang Y, Jung TD, Yoo DS, et al. Diffusion tensor imaging and fiber tractography of patients with cervical spinal cord injury. *J Neurotrauma* 2010;27:2033–40.
5. Assaf Y, Pasternak O. Diffusion tensor imaging (DTI)-based white matter mapping in brain research: a review. *J Mol Neurosci* 2008;34:51–61.

6. Lipton ML, Gellella E, Lo C, et al. Multifocal white matter ultrastructural abnormalities in mild traumatic brain injury with cognitive disability: a voxel-wise analysis of diffusion tensor imaging. *J Neurotrauma* 2008;25:1335–42.
7. Bello L, Gambini A, Castellano A, et al. Motor and language DTI Fiber Tracking combined with intraoperative subcortical mapping for surgical removal of gliomas. *Neuroimage* 2008;39:369–82.
8. van Hecke W, Nagels G, Emonds G, et al. A diffusion tensor imaging group study of the spinal cord in multiple sclerosis patients with and without T2 spinal cord lesions. *J Magn Reson Imaging* 2009;30:25–34.
9. Mori S, Zhang J. Principles of diffusion tensor imaging and its applications to basic neuroscience research. *Neuron* 2006;51:527–39.
10. Demir A, Ries M, Moonen CT, et al. Diffusion-weighted MR imaging with apparent diffusion coefficient and apparent diffusion tensor maps in cervical spondylotic myelopathy. *Radiology* 2003;229:37–43.
11. Facon D, Ozanne A, Fillard P, et al. MR diffusion tensor imaging and fiber tracking in spinal cord compression. *AJNR Am J Neuroradiol* 2005;26:1587–94.
12. Kara B, Celik A, Karadereler S, et al. The role of DTI in early detection of cervical spondylotic myelopathy: a preliminary study with 3-T MRI. *Neuroradiology* 2011;53:609–16.
13. Uchida K, Baba H, Maezawa Y, et al. Progressive changes in neurofilament proteins and growth-associated protein-43 immunoreactivities at the site of cervical spinal cord compression in spinal hyperostotic mice. *Spine (Phila Pa 1976)* 2002;27:480–6.
14. Yamaura I, Yone K, Nakahara S, et al. Mechanism of destructive pathologic changes in the spinal cord under chronic mechanical compression. *Spine (Phila Pa 1976)* 2002;27:21–6.
15. Okawa A, Nakamura I, Goto S, et al. Mutation in Npps in a mouse model of ossification of the posterior longitudinal ligament of the spine. *Nat Genet* 1998;19:271–3.
16. Yu WR, Baptiste DC, Liu T, et al. Molecular mechanisms of spinal cord dysfunction and cell death in the spinal hyperostotic mouse: implications for the pathophysiology of human cervical spondylotic myelopathy. *Neurobiol Dis* 2009;33:149–63.
17. Uchida K, Baba H, Maezawa Y, et al. Histological investigation of spinal cord lesions in the spinal hyperostotic mouse (twy/twy): morphological changes in anterior horn cells and immunoreactivity to neurotropic factors. *J Neurol* 1998;245:781–93.
18. Baltes C, Radzwill N, Bosshard S, et al. Micro MRI of the mouse brain using a novel 400 MHz cryogenic quadrature RF probe. *NMR Biomed* 2009;22:834–42.
19. Bosshard SC, Baltes C, Wyss MT, et al. Assessment of brain responses to innocuous and noxious electrical forepaw stimulation in mice using BOLD fMRI. *Pain* 2010;151:655–63.
20. Ogura H, Matsumoto M, Mikoshiba K. Motor discoordination in mutant mice heterozygous for the type 1 inositol 1,4,5-trisphosphate receptor. *Behav Brain Res* 2001;122:215–9.
21. Kouda K, Iki M, Fujita Y, et al. Alcohol intake and bone status in elderly Japanese men: baseline data from the Fujiwara-kyo osteoporosis risk in men (FORMEN) study. *Bone* 2011;49:275–80.
22. Yu WR, Liu T, Kiehl TR, et al. Human neuropathological and animal model evidence supporting a role for Fas-mediated apoptosis and inflammation in cervical spondylotic myelopathy. *Brain* 2011;134:1277–92.
23. Baba H, Imura S, Kawahara N, et al. Osteoplastic laminoplasty for cervical myeloradiculopathy secondary to ossification of the posterior longitudinal ligament. *Int Orthop* 1995;19:40–5.
24. Iwasaki M, Okuda S, Miyauchi A, et al. Surgical strategy for cervical myelopathy due to ossification of the posterior longitudinal ligament: Part 2: Advantages of anterior decompression and fusion over laminoplasty. *Spine (Phila Pa 1976)* 2007;32:654–60.
25. Sakai K, Okawa A, Takahashi M, et al. 5-year follow-up evaluation of surgical treatment for cervical myelopathy caused by ossification of the posterior longitudinal ligament: a prospective comparative study of anterior decompression and fusion with floating method versus laminoplasty. *Spine (Phila Pa 1976)* 2012;37:367–76.
26. Iwasaki M, Okuda S, Miyauchi A, et al. Surgical strategy for cervical myelopathy due to ossification of the posterior longitudinal ligament: part 1: clinical results and limitations of laminoplasty. *Spine (Phila Pa 1976)* 2007;32:647–53.
27. Tani T, Ushida T, Ishida K, et al. Relative safety of anterior microsurgical decompression versus laminoplasty for cervical myelopathy with a massive ossified posterior longitudinal ligament. *Spine (Phila Pa 1976)* 2002;27:2491–8.
28. Fujiyoshi K, Yamada M, Nakamura M, et al. In vivo tracing of neural tracts in the intact and injured spinal cord of marmosets by diffusion tensor tractography. *J Neurosci* 2007;27:11991–8.
29. Takagi T, Nakamura M, Yamada M, et al. Visualization of peripheral nerve degeneration and regeneration: monitoring with diffusion tensor tractography. *Neuroimage* 2009;44:884–92.
30. Mamata H, Jolesz FA, Maier SE. Apparent diffusion coefficient and fractional anisotropy in spinal cord: age and cervical spondylosis-related changes. *J Magn Reson Imaging* 2005;22:38–43.
31. Baba H, Maezawa Y, Imura S, et al. Quantitative analysis of the spinal cord motoneuron under chronic compression: an experimental observation in the mouse. *J Neurol* 1996;243:109–16.
32. Yato Y, Fujimura Y, Nakamura M, et al. Decreased choline acetyltransferase activity in the murine spinal cord motoneurons under chronic mechanical compression. *Spinal Cord* 1997;35:729–34.

TECHNICAL NOTE doi: 10.2176/nmc.tn2012-0223

Neurol Med Chir (Tokyo) 53, 907–913, 2013 Online October 7, 2013

Novel Method for Analyzing Locomotor Ability after Spinal Cord Injury in Rats: Technical Note

Munehisa SHINOZAKI,[1,2] Akimasa YASUDA,[3] Satoshi NORI,[3] Nobuhito SAITO,[2] Yoshiaki TOYAMA,[3] Hideyuki OKANO,[1] and Masaya NAKAMURA[3]

Departments of [1]Physiology and [3]Orthopedic Surgery, Keio University School of Medicine, Tokyo; [2]Department of Neurosurgery, Graduate School of Medicine, University of Tokyo, Tokyo

Abstract

In the research for the treatment of spinal cord injury (SCI), the evaluation of motor function in model rats must be as objective, noninvasive, and ethical as possible. The maximum speed and acceleration of a mouse measured using a SCANET system were previously reported to vary significantly according to severity of SCI. In the present study, the motor performance of SCI model rats was examined with SCANET and assessed for Basso-Beattie-Bresnahan (BBB) score to determine the usefulness of the SCANET system in evaluating functional recovery after SCI. Maximum speed and acceleration within the measurement period correlated significantly with BBB scores. Furthermore, among several phased kinematic factors used in BBB scores, the capability of "plantar stepping" was associated with a drastic increase in maximum speed and acceleration after SCI. Therefore, evaluation of maximum speed and acceleration using a SCANET system is a useful method for rat models of SCI and can complement open field scoring scales.

Key words: acceleration, locomotor ability, hindlimb function, speed, spinal cord injury

Introduction

Open field scores such as the Basso-Beattie-Bresnahan (BBB) score for rats[1] and Basso Mouse Scale (BMS) for mice[2] are widely used as simple and reliable methods for evaluating motor performance after spinal cord injury (SCI) in rodents. However, eliminating subjectivity from these methods requires assessment by multiple skilled examiners in a blinded manner. In addition, since these ratings are not linear, the potential for quantitative comparison or analysis of scores is limited.[7] A complementary objective method is thus indispensable.

We previously reported the usefulness of the SCANET system, with which an animal can be evaluated easily, noninvasively, and reproducibly.[4,5] Maximum speed and acceleration calculated from raw data obtained by SCANET effectively distinguished between a thoracic transection model, a contusion model, and uninjured mice.[8] Nevertheless, the previous reports leave several concerns. First, the effectiveness of the SCANET on rats has not been demonstrated. The length of each side of the box in the system is 45 cm, which limits the running space for a rat compared to that of a mouse under the same condition. Whether a rat is capable of reaching top speed and demonstrating its best performance is unclear. Next, in the contusion model, although a correlation between open field score and maximum speed was suggested in a prior study,[8] the data may have reflected only the natural recovery process, because longitudinal data were included for the calculation of the correlation coefficient. To describe the correlation more precisely, data should be examined at each time point. Third, the superiority of the SCANET to other methods has not been determined. The key advantage of the SCANET is its ability to evaluate an animal at the time of its best performance, whereas other examinations are performed at an arbitrary time. Therefore, the invalidity of evaluating an animal at an arbitrary time should also be demonstrated.

To address these issues, we used contusion-model rats to evaluate the correlation between open field score and maximum speed/acceleration at each time point until 6 weeks after injury. Average speed was calculated as the performance at an arbitrary time and also compared to open field score. We further

Received June 12, 2012; Accepted August 30, 2012

examined the locomotive factors used to determine open field scores for an in-depth investigation of their relationships with maximum speed/acceleration.

Materials and Methods

I. SCI

The present study used 35 6-week-old adult female Sprague-Dawley rats (body weight, 152–174 g). Animals were anesthetized by intraperitoneal injection of ketamine and xylazine, and the dorsal surface of the dura mater at the T10 level was exposed by laminectomy. Severe contusion SCI was induced in each rat using an IH impactor (Precision Systems and Instrumentation; impact force 250 kdyn), as reported previously.[3,9] The muscles and skin were closed in layers, and the animals were placed in a temperature-controlled chamber until thermoregulation was reestablished. Manual voiding of the bladder was performed twice daily until reflex bladder emptying was reestablished. All experiments and procedures in our study were approved by the Keio University Animal Research Committee in accordance with the Laboratory Animal Welfare Act, the Guide for the Care and Use of Laboratory Animals (National Institutes of Health, Bethesda, Maryland, USA), and the Guidelines and Policies for Animal Surgery provided by the Animal Study Committees of the Central Institute for Experimental Animals and of Keio University.

II. Behavioral analyses

The SCANET MV-40 (MELQUEST, Toyama) is a device that allows behavioral analysis of an animal using high-density-arranged infrared sensors. The infrared sensors are distributed in all directions at 6-mm intervals parallel to the floor of a transparent 45 × 45-cm box. The animal can move freely on the floor. These movements are detected by the infrared sensors, and the coordinates of the center of the animal are recorded on a computer every 0.1s. The height of the sensor from the floor was set at 4 cm. One animal at a time was placed in the box, and after waiting for 10s until the animal settled down, its coordinates were recorded for 5 minutes, as reported previously.[8] Measurement was performed in the same environment before SCI, 1 day after SCI, and weekly until 6 weeks postoperatively.

Motor function of the hindlimbs in each rat was also evaluated using BBB score. Individual animals were allowed to move freely for 5 minutes, and hindlimb movements were observed by two examiners. The average score was used as the recorded value.

III. Data analysis

The distance moved every 0.1 s was calculated as speed (m/s) for each interval of time. Next, the rate of change in speed per 0.1 s was calculated as acceleration (m/s^2) for each interval of time. Example data are shown in Table 1. Since the coordinate per unit in raw data was equivalent to 6 mm, the formulae were as follows:

$$D_n = [(X_{n+1} \times 0.006 - X_n \times 0.006)^2 + (Y_{n+1} \times 0.006 - Y_n \times 0.006)^2]^{0.5} \text{ (m)},$$

$$S_n = D_n/0.1 \text{ (m/s)},$$

$$A_n = (S_{n+1} - S_n) / 0.1 \text{ (m/s}^2\text{)},$$

where X_n, Y_n, D_n, S_n, and An are the x and y coordinates, moving distance, speed, and acceleration, respectively, at a time point n. Maximum speed and maximum acceleration over 5 minutes were extracted as the real performance of each animal. Maximum deceleration was also calculated as an indicator of braking performance of the animal. Moreover, the average speed during movement was computed as the total distance moved by each animal divided by its total time spent moving.

Table 1 Example of data for coordinates, speed, and acceleration

Time	X	Y	Distance (m)	Speed (m/s)	Acceleration (m/s^2)
.	.	.	.	.	.
.	X_n	Y_n	.	.	.
.	X_{n+1}	Y_{n+1}	D_n	S_n	.
.	.	.	.	S_{n+1}	A_n
34.31.0	60	38	.	.	.
34.31.1	60	38	0	0	.
34.31.2	60	39	0.006	0.06	0.6
34.31.3	59.5	44.5	0.0331361	0.331361	2.71361
34.31.4	59	50	0.0331361	0.331361	0
34.31.5	58.5	50	0.0067082	0.067082	−2.6428
34.31.6	58.5	50	0	0	−0.67082
.	.	.	.	.	.

Raw serial data of time and X–Y coordinates for a 0.6-s epoch are shown. Data are recorded every 0.1 s, so 3000 rows are recorded in 5 minutes in practice. Speed and acceleration were calculated using our custom program (see text for formulae). For this 0.6-s epoch, maximum speed is 0.33 m/s, and maximum acceleration is 2.71 m/s^2.

IV. Statistical analysis

All values are reported as means ± standard error of the mean. The strength of correlation between each parameter and BBB score was determined using the Pearson correlation coefficient.

Results

I. Speed and acceleration correlate significantly with open field scores

The time courses of BBB scores are shown in Fig. 1. BBB scores were 0 at Day 1 after SCI and gradually recovered to plateau around five points, as reported previously.[6]

Maximum speed gradually recovered from 0.33 m/s at 1 day to 0.48 m/s at 42 days after SCI. Likewise, maximum acceleration recovered from 2.7 m/s^2 to 3.76 m/s^2 (Fig. 1). Correlation coefficients between BBB scores and maximum speed were 0.22 ($p = 0.21$) at 1 week, 0.35 ($p < 0.05$) at 2 weeks, 0.54 ($p < 0.001$) at 3 weeks, 0.65 ($p < 0.0001$) at 4 weeks, 0.43 ($p < 0.01$) at 5 weeks, and 0.58 ($p < 0.001$) at 6 weeks after SCI. Significant relationships were found from 2 to 6 weeks. Similar to maximum speed, significant correlations between BBB scores and maximum acceleration were observed from 1 week to 6 weeks. Correlation coefficients were 0.35 ($p < 0.05$) at 1 week, 0.39 ($p < 0.05$) at 2 weeks, 0.50 ($p < 0.01$) at 3 weeks, 0.53 ($p < 0.001$) at 4 weeks, 0.50 at 5 weeks ($p < 0.01$), and 0.63 ($p < 0.0001$) at 6 weeks after SCI. Representative diagrams are shown in Fig. 2. The maximum speed and maximum acceleration using data from each time point correlated significantly with hindlimb function in SCI model rats.

II. In severe SCI models, maximum speed and acceleration are higher in animals capable of plantar stepping

BBB scoring is based on several kinematic factors. However, few previous reports have clarified the relative importance of each factor to evaluate hindlimb functions. We therefore examined the relationships between maximum speed and acceleration and the factors "ankle extension," "weight support," and "plantar stepping" from the longitudinal data of all rats. Relationships between each category and hindlimb status were defined as follows: none, ankle extension impossible on either or both hindlimbs ($n = 148$); ankle extension, ankle extension possible on both hindlimbs, but not weight support ($n = 66$); weight support, weight support possible, but frequent to consistent plantar stepping impossible on either or both hindlimbs ($n = 14$); and plantar stepping, frequent to consistent plantar stepping possible on both hindlimbs ($n = 7$). Maximum speed and acceleration were dramatically increased in animals capable of plantar stepping (Fig. 3), suggesting plantar stepping as the most important locomotive factor in severe SCI model rats.

III. Braking performance depends on hindlimb ability in SCI model rats

To evaluate locomotor ability, braking performance should also be addressed. However, no previous reports have examined braking performance in rodents after SCI. Braking performance is expressed as a decrease in speed, that is, deceleration. We extracted maximum deceleration from the acquired data. Representative scatter diagrams of maximum deceleration and BBB scores are shown in Fig. 4. A significant correlation was observed between braking performance and BBB scores, with correlation coefficients of −0.35 ($p < 0.05$) at 1 week, −0.35 ($p < 0.05$) at 2 weeks, −0.48 ($p < 0.01$) at 3 weeks, −0.43 ($p < 0.01$) at 4 weeks, −0.47 ($p < 0.01$) at 5 weeks, and −0.58 ($p < 0.001$) at 6 weeks. Moreover, braking performance improved in animals with plantar stepping compared with other kinematic factors, suggesting that braking

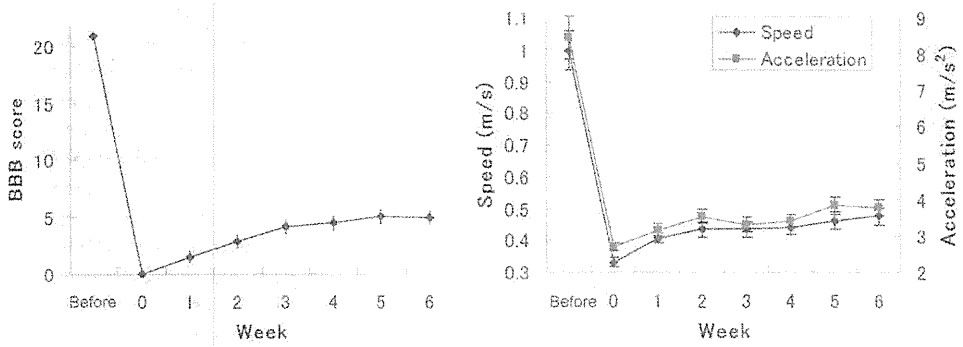

Fig. 1 Time course of Basso-Beattie-Bresnahan (BBB) scores, maximum speed, and maximum acceleration for rats. (*Left*) Rats scored near zero at Day 1 after spinal cord injury (SCI), with subsequent gradual recovery: most reached a plateau after 3 weeks. (*Right*) Both maximum speed and maximum acceleration gradually recovered and reached a plateau within 3 weeks after SCI.

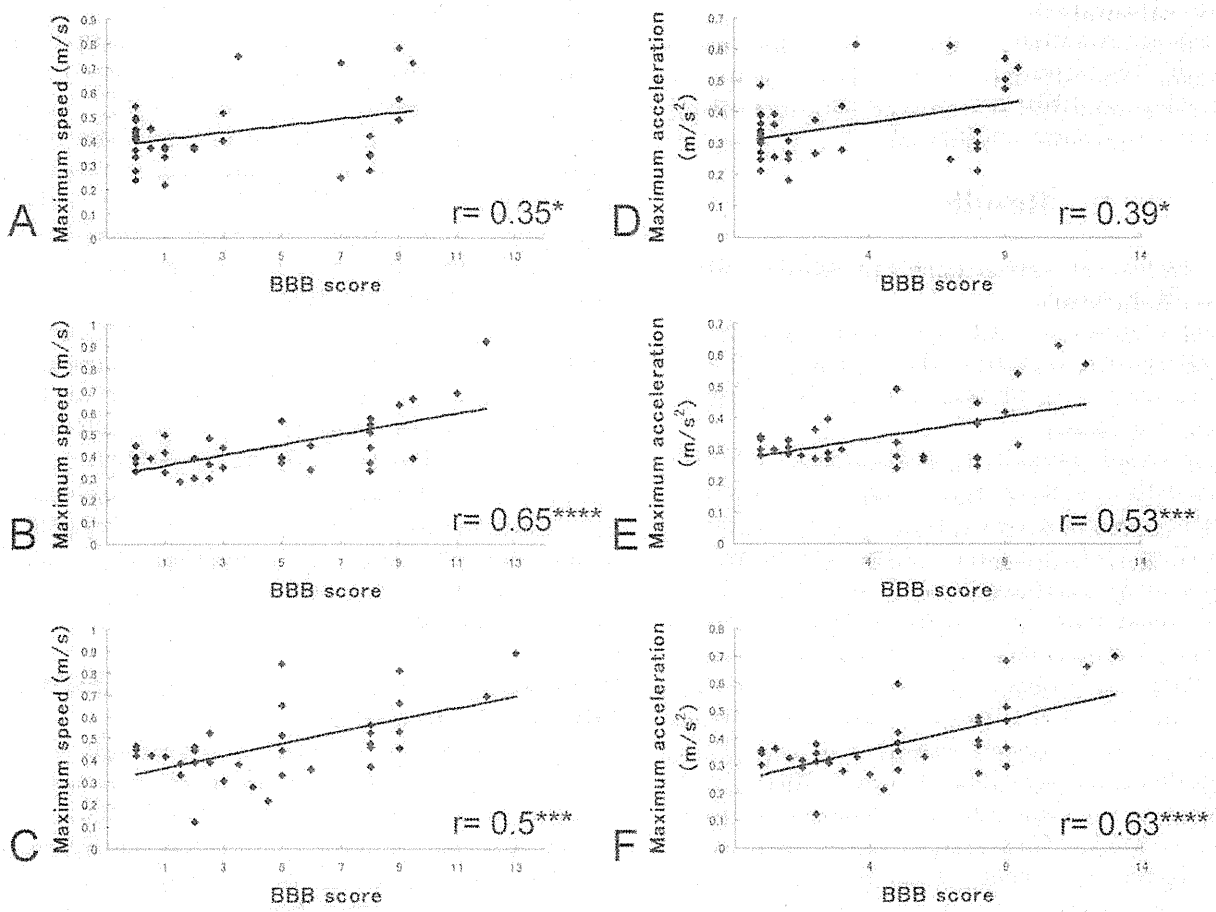

Fig. 2 Correlation between Basso-Beattie-Bresnahan (BBB) scores and maximum speed and acceleration. A–C: Scatter diagrams of BBB scores and maximum speed at 2, 4, and 6 weeks after spinal cord injury (SCI). The distribution of BBB scores shifted as time advanced, but a significant correlation was preserved. D–F: Scatter diagrams of BBB scores and maximum acceleration at 2, 4, and 6 weeks after SCI, respectively. A significant correlation was again apparent. *$p < 0.05$, ***$p < 0.001$, ****$p < 0.0001$.

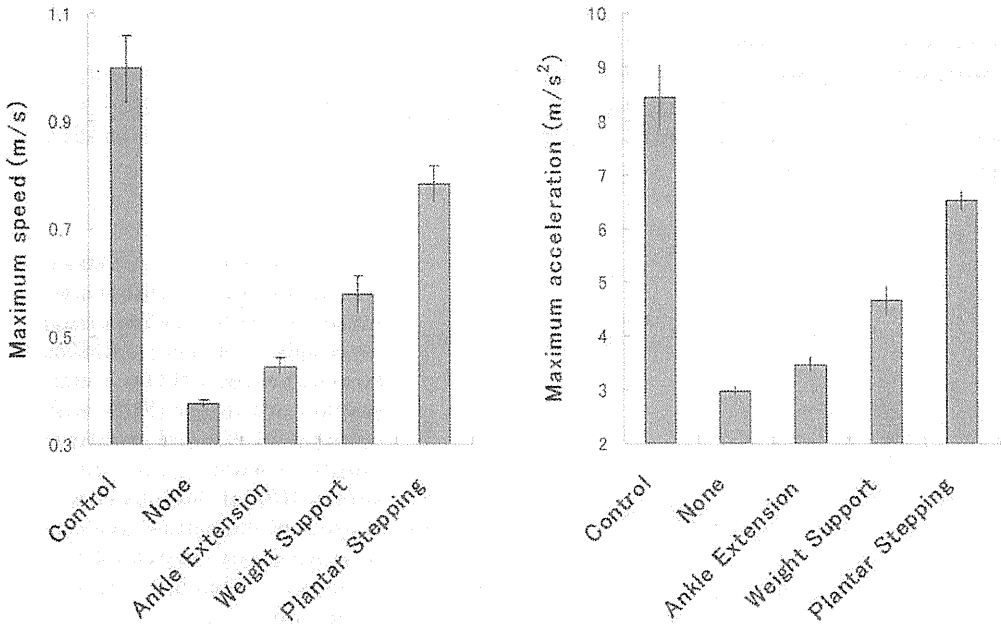

Fig. 3 Relationship between kinematic factors and maximum speed or acceleration. (*Left*) The relationship between maximum speed and kinematic factors of the Basso-Beattie-Bresnahan (BBB) score. Maximum speed demonstrated a stepwise increase with improved factors. "Plantar stepping" was associated with a dramatic increase in maximum speed. (*Right*) The same tendency was observed for maximum acceleration. Statistical analysis was not performed, because these data are longitudinal.

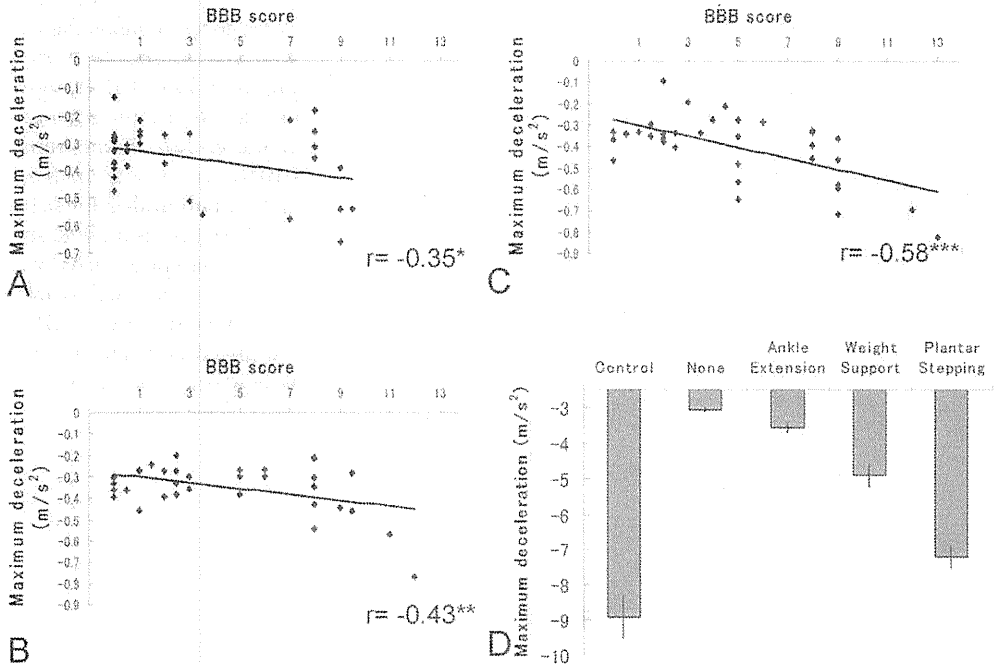

Fig. 4 Characteristics of braking ability. A–C: Representative scatter diagrams of Basso-Beattie-Bresnahan (BBB) scores and maximum deceleration at 2, 4, and 6 weeks after spinal cord injury (SCI). Significant correlations were observed for all time periods. D: Relationship between braking ability and kinematic factors. Similar to maximum speed and acceleration, braking ability increased markedly with the presence of "Plantar stepping." *p < 0.05, **p < 0.01, ***p < 0.001.

performance also depends on hindlimb function in SCI model rats.

IV. Performance at an arbitrary time point does not reflect motor function

As an animal may move vigorously at one time and barely move at another time, speed and acceleration are always variable. Therefore, when an examiner evaluates movement performance using arbitrary timing, the results may not reflect true motor function. To investigate this possibility, we calculated average speed (total distance moved divided by total time spent moving) and compared it with BBB score, under the assumption that locomotor ability reflected hindlimb function. Indeed, average speed was reduced from 0.13 m/s to 0.06 m/s with loss of hindlimb function, and showed a stepwise increase with improved factors (Fig. 5). However, no significant correlation was found between average speed and BBB score. Accurate hindlimb performance thus could not be determined when measurement was executed using arbitrary timing, even if the animal was voluntarily moving as the examiner intended.

Discussion

Locomotion of rats is performed using both forelimbs and hindlimbs. If the hindlimbs are impaired, locomotor ability declines, but a long distance can still be moved using only the forelimbs, given sufficient time. Hence, to assess locomotor ability, the examiner should consider the distance moved per unit time, that is, speed. Furthermore, since speed determined over an arbitrary time period does not always reflect hindlimb function, the best performance should be extracted. From another perspective, locomotor ability is dependent on the force to move, and force can be determined by acceleration, assuming a constant mass of the animal. The present study revealed that maximum speed and maximum acceleration in severe SCI model rats bear significant relationships to BBB scores, which essentially focus on hindlimb functions rather than locomotor ability.

The most serious problem with existing behavioral evaluations for rats is noncooperation, and the performance of an animal does not always reflect maximal ability. Most examinations including the inclined test, grid walk, beam walk, and manual footprint analysis require the cooperation of the animal to perform the tested motion. However, since we found that performance at an arbitrary time point bears no relationship to hindlimb function, those motions are not guaranteed to reflect the best performance. To use these examinations, several sessions must be carried out, and the best result should be used.

Simplicity is also required for repeated examinations over time. Automatic footprint or kinematic